JOURNAL OF GEOPHYSICAL RESEARCH, VOL. 94, NO. B8, PAGES 10,279–10,298, AUGUST 10, 1989

Slip Patterns in a Spatially Homogeneous Fault Model

FRANKLIN G. HOROWITZ[1]

Department of Geological Sciences, Cornell University, Ithaca, New York

ANDY RUINA

Department of Theoretical and Applied Mechanics, Cornell University, Ithaca, New York

We present a model which predicts seismological complexity even with no complexity in geometry or heterogeneity in material properties. Fault slip is numerically modeled using a Dieterich-type rate and state variable friction law at the planar interface of two infinitely long massless elastic slabs. A constant velocity boundary condition is imposed a distance H from each interface. No geometrical, frictional, elastic, or remote loading variations are allowed in the direction parallel to the plane of the fault. In the numerical solution a periodic boundary condition is imposed, and the fault surface is divided into N subregions each of which is represented by a mathematical point. At these N points, all of which are mutually coupled by discretized two-dimensional elasticity solutions, the friction law differential equations are numerically solved. The character of the solutions depends on model parameter values and initial conditions. Solutions are found that are periodic, quasi-periodic, or aperiodic in time; and that are spatially homogeneous for all time, nearly homogeneous except during fast slip events, or essentially inhomogeneous for all time. For given parameter values the solutions have a qualitative character which is nearly independent of initial conditions. At any instant in time these solutions ultimately appear roughly as some superposition of those spatial sine waves which are unstable in a linearized calculation. When spatially complex, the solutions can simultaneously exhibit regions that have steady sliding, large slip rates, and local propagating creep events. Special initial conditions can generate other solutions such as steady propagating creep waves that span the whole fault. The variety of simulated slip motions and long-term patterns of slip predicted by this spatially homogeneous nonlinear dynamical model suggests a possible role for dynamics, and not just complex geological structure, as a generator of temporal and spatial complexity in seismic phenomena.

INTRODUCTION

It is natural to assume that seismic activity is complex because the Earth is complex. Fault traces meander and cross, mechanical properties of faults and their adjoining crust are heterogeneous, and fault loading may be due to erratic tectonic processes. But some aspects of seismic patterns may follow from the dynamics of the slip process to the extent that they would be maintained even if all complexity in the Earth's structure were eliminated. The possibility of complexity in a simple dynamical earthquake model is suggested by the complicated motions observed in the one-degree-of-freedom spring block calculations of *Ruina* [1983] and *Gu et al.* [1984] and by the lack of spatial symmetry in the solutions of the symmetric two-block model of *Nussbaum and Ruina* [1987]. Complexity has also been observed in solutions of models with many rigid blocks coupled with elastic springs using a variety of friction laws. To our knowledge all of these multiblock models, excepting *Nussbaum and Ruina* [1987], impose some spatial variation in properties or boundary conditions. But such complex boundary conditions may not be the only reason for spatial patterns in seismic response. One may use turbulent fluid flow as a suggestive analogy [e.g., *Andrews*, 1978]. Fluid flow can be complex even when the boundaries of flow are smooth, as in the fast flow of water in a straight pipe.

To emphasize the possible role of dynamics in generating seismic complexity, we have begun to investigate the spatially heterogeneous motions predicted in a simple fault model that has no spatial heterogeneity in properties. The fault is treated as a continuum, although for numerical purposes it is discretized in a manner that makes the model formally equivalent to a multiple spring block model. The model in some ways generalizes single spring block models as well as the linearized continuum analysis of *Rice and Ruina* [1983]. The calculation methods used are similar to those used by *G.M. Mavko* [1980, 1983] (and unpublished manuscript, 1984). The 10-block model of *Cao and Aki* [1986] is quite similar, in that a similar friction law is used, but those authors do not produce solutions to a continuum model, and they also explicitly impose heterogeneous properties.

The Plan of the Paper

The presentation is organized as follows. After some definitions and comments about the model in general physical terms, we present a detailed discussion of the friction law. As motivation for the nonlinear continuum problem here, we then present some results from nonlinear spring block studies. The details of the elasticity equations and a summary of the full set of governing equations are then presented, followed by a discussion of the periodic bound-

[1] Now at Department of Civil Engineering, Northwestern University, Evanston, Illinois.

Paper number 88JB03739.
0148-0227/89/88JB-03739$05.00

ary conditions and the symmetries that they preserve. The linearized-continuum and spring block results are next used to make definite statements and to motivate speculations about the full nonlinear continuum solutions. Next and most significantly, numerical solutions are presented with some observations and comments. Finally we make some observations about the solutions and speculations based on these observations. For reference, appendices contain discussions of some dynamics terminology (especially the word 'instability') and the numerical method. Definitions of all variables and constants are given in a notation section.

Slip or Strain

At a large scale the displacement jump observed across the boundaries of neighboring tectonic plates may be thought of as slip. For the purposes of large-scale earthquake modeling one might apply some friction law to this macroscale slip, encompassing deformation or faulting within the fault zone as a micromechanism. But this macroslip may be closely related to what would be called slip at a human or laboratory scale, at least during earthquakes. Seismic and geodetic data are often well fit to a model of slip on a surface or surfaces, although not to a resolution of millimeters. But excavations by, for example, ***Weldon and Sieh*** [1985] support the notion that the shear deformation during earthquakes may localize to a scale of millimeters or less, though the applicability of these surface observations to subsurface slip is not assured.

Last, it seems to be a general rule that any local (i.e., stress-strain) continuum deformation law which can explain the possibility of the sudden release of elastic energy also predicts localization of deformation to a surface and hence the inapplicability of that law. These continuum shear deformation laws predict their own demise by localization as or before they predict sudden motions. Such deformation laws include those where stress is a function of strain, where stress is a function of strain rate, and where stress is related to strain by a rate and state law of the type that we shall employ for stress as a function of slip displacement.

So to model instabilities in a fault zone one may assume that (1) the deformation is by slip, (2) the deformation in the fault zone is by some kind of cataclastic flow which cannot be described as a smooth deformation, or that (3) this cataclastic flow can be described on average, at the macroscale, by a slip law. Although the friction law that we use is motivated by assumption 1, general aspects of our results may apply to models based on assumption 3 as well.

Macroscopic Model of Crustal Loading

There is general agreement that the upper lithosphere is largely elastic over the time scale of interest, so an elastic model for the solid material adjoining the fault is employed here, as in most earthquake models.

For definiteness, we think of our model as being the straight strike-slip fault shown in Figure 1*a*. Even though the driving forces for plate motion may be distributed over large regions of the plate, we assume regions at a distance H from the slip surface move at a constant relative displacement rate, unaffected by erratic seismic slip. The viscouslike process which restricts diffusion of earthquake related deformation into the plate may be an increase in the viscosity of the friction relation with depth, as discussed by G.M. Mavko (unpublished manuscript, 1984) and ***Tse and Rice*** [1986], or

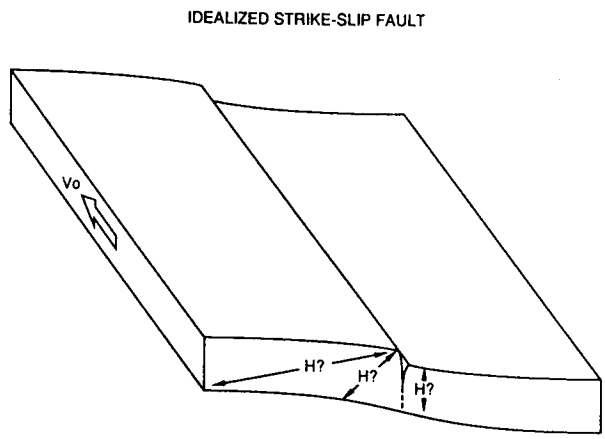

Fig. 1*a*. View of the physical problem. Strike slip fault in the lithosphere. Remote tectonic loading is coupled with both the active fault and viscous processes near the active fault. At a distance H from the active fault the displacement rate is nearly constant independent of earthquake activity.

may be due to viscous deformation of the asthenosphere. Our crude approximation is that there is a finite distance H inside which viscous effects can be neglected and outside which the motion may be considered rigid. We also simply assume that remote tectonic processes are constant over the time scale of our model (many earthquake cycles). Thus we are led to the boundary condition of a constant rate V_0 at a distance H.

Since we are interested in looking at models with the same physical conditions imposed at every spatial point, we look for solutions that vary horizontally along strike. We thus neglect the pressure and material property variations with depth which were the focus of study by G.M. Mavko (unpublished manuscript, 1984), ***Tse and Rice*** [1986], and ***Stuart*** [1988]. A two-dimensional representation of the fault model is shown in Figure 1*b*.

FRICTION LAWS

Tullis [1987] briefly discusses the open question of whether any of the friction behaviors observed in any of several laboratories apply to the slip or cataclastic flow in an interplate fault zone. An applicable friction law must have certain features. Many of these features are in the state variable friction laws of the general type first proposed by ***Dieterich*** [1979*a*, 1981]. Further experimental and heuristic motivation for use of such laws is given by, for example, ***Dieterich*** [1979*b*], ***Dieterich and Conrad*** [1984], ***Ruina*** [1983, 1984], ***Tullis*** [1987], and ***Tse and Rice*** [1986].

Earthquake Applicable Friction Laws

In order to simulate seismicity patterns the friction law used must be capable of producing sudden slip events and also must be sensible in the mechanical model that is being used. For the purposes of an elastic continuum seismicity pattern model, the most important requirements for the friction law are the following:

1. In at least some circumstances the friction stress must decrease as the slip rate transiently increases (softening behavior). In systems with constant normal stress, some kind of softening is necessary for there to be sudden slip.

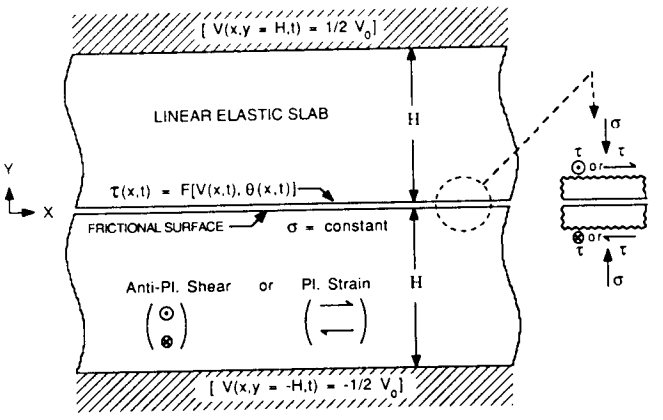

Fig. 1b. Elastic slab model. The frictional surfaces see rigid boundary conditions at a distance H, where the displacement rate is constant. The elasticity is modeled as plane strain or antiplane shear.

2. Healing must be possible after a slip event so that there can be another.

3. When the slip rate is instantaneously increased, the friction stress must not decrease instantaneously but transiently over some slip distance. For example, an instantaneous jump would occur if friction stress were to (negatively) depend only on the instantaneous slip rate. Such a law is probably senseless on the boundary of a deformable elastic solid since it unconditionally leads to instantaneous growth of spatial perturbations as follows from the analysis of *Rice and Ruina* [1983]. The use of two distinct coefficients of friction, static and dynamic, also leads to such jumps and is also problematic on the boundary of a continuum [*Ruina*, 1984].

State Variable Friction Laws

The state variable friction laws used since the work by *Dieterich* [1979a] satisfy the needs named above while also fitting some laboratory observations of rock friction, particularly experiments in which the slip rate is controlled to suddenly change from one value to another. In these friction laws the friction stress τ depends on the normal stress σ, the slip rate V, and the surface state θ. In these relations, θ is a state variable which is a measure of the evolving quality of surface contact. *Dieterich and Conrad* [1984] present evidence for a possible microscopic interpretation for a state variable θ. But even without rigorous microscopic justification, one can write laws for the evolution of the state θ that allow one to fit aspects of experimental data.

Experimental Data

Experimental results with polished quartzite at low normal stress are shown in Figure 2a. In these experiments the slip speed is servocontrolled to be piecewise constant at a range of rates with the normal stress held constant. Friction stress τ is plotted against slip displacement as these jumps in slip rate are imposed.

Features of these data that we note before choosing a specific form for a constitutive law are these (not all of which are precisely observed in all experiments) [*Dieterich*, 1979a; *Ruina*, 1983]:

1. When the slip rate jumps up, the friction stress jumps an amount about proportional to the log of the ratio of the postjump to prejump slip rates. Similarly, the friction stress jumps down when the slip rate jumps down.

2. After the friction stress τ jumps up at a step increase in slip rate, it relaxes to a lower level. The amount of net change in friction stress long after this jump is also about proportional to the log of the ratio of the slip rates.

3. The transient in τ that occurs at step changes in slip rate has a characteristic distance that is independent of slip rate.

The ultimate, posttransient level of friction stress at a given slip rate is assumed to depend only on the slip rate, and not the slip history. One can thus discuss a steady state friction relation $\tau_{ss}(V)$, even though such constant rate slip might never occur on a fault surface. Since the friction stress in Figure 2a ultimately drops after an increase in slip rate, we have that $d\tau_{ss}/dV < 0$ for these experiments.

The Friction Law

For the transients shown in Figure 2a to be accurately predicted with a state variable friction law would require at least two state variables [*Ruina*, 1983]. For simplicity we approximate the transient change as an exponential decay so that a single state variable can be used.

The particular state variable friction law that we use (equations (1a) and (1b) below) is very close to the law used by *Tse and Rice* [1986], which is in turn a slight modification of the law proposed by *Ruina* [1983] as an approximation to that of *Dieterich* [1979a].

$$\tau = F(V,\theta) = \sigma\left(\mu_0 + \theta + A\ln\left(\frac{V}{V_t}\right)\right) \tag{1a}$$

$$\frac{d\theta}{dt} = G(V,\theta) = -\frac{V}{d_c}\left(\theta + B\ln\left(\frac{V}{V_t}\right) + C\ln\left(\frac{V}{V+V_t}\right)\right) \tag{1b}$$

from which it follows, as explained below, that

$$\tau_{ss} = \sigma\left(\mu_0 + (A-B)\ln\left(\frac{V}{V_t}\right) - C\ln\left(\frac{V}{V+V_t}\right)\right) \tag{1c}$$

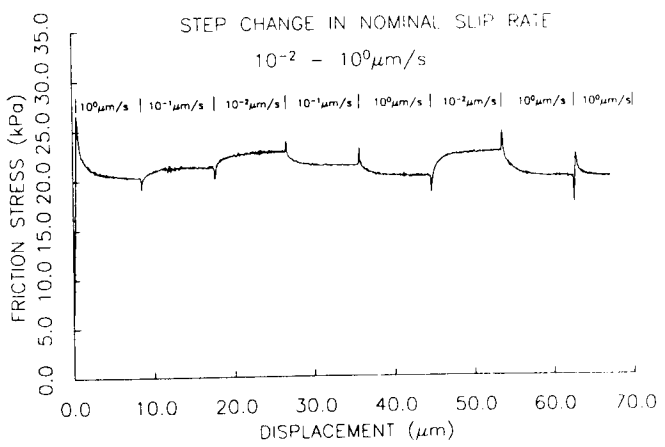

Fig. 2a. Experimental data showing friction stress versus slip displacement at step changes in slip rate with fine-grained quartzite. The slip rate is increased and decreased by factors of 10 and 100.

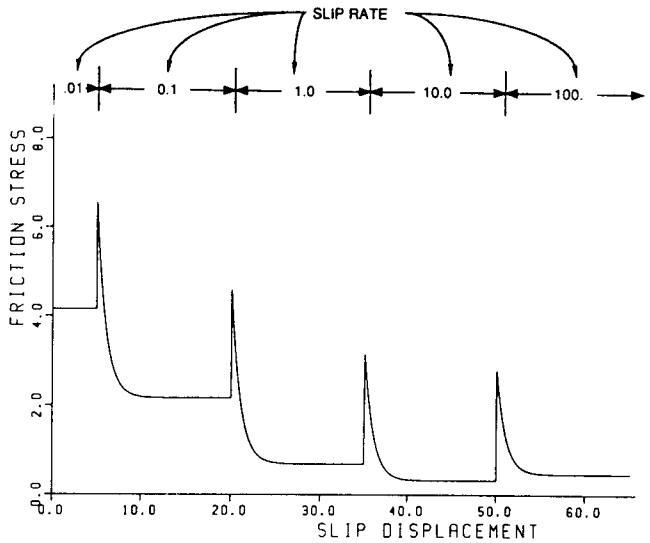

Fig. 2b. Simulated data using the friction law (1). The simulation assumes slip rate is controlled to be piecewise constant through a stiff (but not rigid) machine. Slip rate of 1 ($\log(V) = 0$) corresponds to $V = V_t = V_0$ in our simulations (where $V_0 = V_t$).

where t is time and A, B, C, d_c, V_t, and μ_0 are positive material constants. When $A = B$, (1) reduces to the law used by *Tse and Rice* [1986] and by *Stuart* [1988].

The τ_{ss} in (1c) is the steady state shear stress for sliding at constant speed V; τ_{ss} can be found from (1a) and (1b) by setting $d\theta/dt = 0$ in (1b), solving for θ in terms of V, using this result in (1a) and then defining $\tau_{ss} \equiv \tau$.

With (1), both softening during accelerating slip and rehealing when slip slows follow from transient changes in the state variable θ, governed by the evolution equation (1b). These are properties of many possible state variable friction laws [*Ruina*, 1983]. Predictions of the law (1), with A=1.1, B=C=1, d_c=1, and V_t=1, are illustrated in Figures 2b and 2c. Figures 2b and 2c show the friction stress versus slip displacement and versus slip rate for a sequence of step changes in slip rate. A feature of the friction law (1) (Figures 2b and 2c), not supported by the experimental data of Figure 2a, is a change in $d\tau_{ss}/dV$ from negative to positive with increasing V. This feature shows in Figure 2b as the positive change in friction stress when the slip rate is changed from 10 to 100 and as the positive slope of the dash-dotted line for large slip rate (Figure 2c). This feature has been incorporated in (1) by adding one term to *Ruina's* [1983] approximation to the law of *Dieterich* [1979a]. This term includes two constants: C and V_t. For nonzero C, V_t is related to the transition speed at which the steady state friction stress ceases to decrease with slip rate (with the parameters we use the transition occurs at about $2V_t$). At low speeds, ($V \ll V_t$), $d\tau_{ss}/d(\ln V)$ is $(A - B - C)$, and at high speeds, ($V \gg V_t$), $d\tau_{ss}/d(\ln V)$ is $(A - B)$.

Our first numerical experiments used C=0. In this case, (1) reduces to the simple approximation of *Dieterich's* [1979a] friction law presented by *Ruina* [1983] and studied extensively by *Gu et al.* [1984]. However, the simplification $C = 0$ (and $B > A$) causes a massless spring block to eventually slide at an infinite rate, precluding numerical simulation of multiple earthquake cycles. These unbounded slip rates were avoided in the spring block models of *Rice and Tse* [1986] and *Cao and Aki* [1986] by the explicit inclusion of inertia. The problem has also been avoided in numerical continuum simulations by *Mavko* [1980, 1983, also unpublished manuscript, 1984], *Dieterich* [1979b, 1981], *Tse and Rice* [1986], and *Stuart* [1988] by not strictly satisfying all the friction and elasticity equations at high speeds.

Using $B + C > A$ (velocity weakening at low speeds) allows instability of steady sliding. Using $A > B$ (velocity strengthening at high speeds) prevents unbounded slip rates in our simulations without the difficulties of including inertia directly in the mechanics. $A > B$ also can be motivated by some experimental observations [e.g., *Blanpied et al.*, 1987].

SINGLE-SPRING-BLOCK MODELS

The spatially dependent solutions that we present are best understood with awareness of the dynamics of a simpler but related model: a single rigid block loaded by constant rate motion (V_0) at one end of a spring and retarded by state variable friction. *Gu et al.* [1984], *Ruina* [1983], *Rice and Ruina* [1983], and others have studied the motions that rate-and-

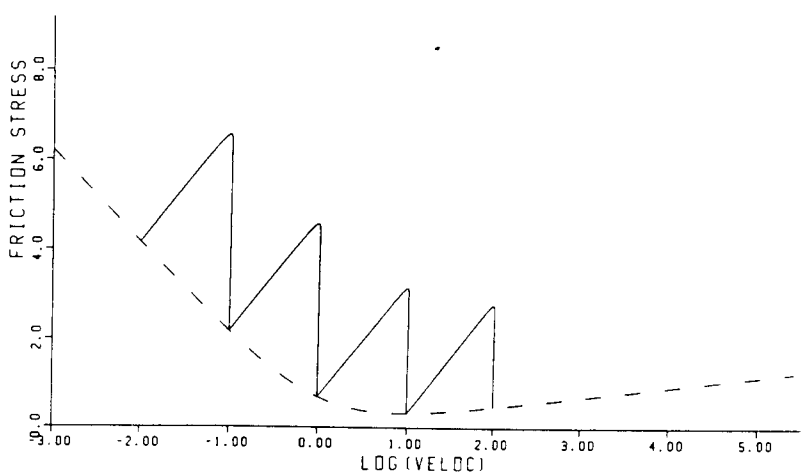

Fig. 2c. Another plot of the simulation of Figure 2b. Friction stress versus slip velocity is shown as well as the steady state dependence of friction force on slip rate (dash-dotted curve).

state friction laws predict for a spring block (spring slider) model. The primary and initially surprising result is that oscillations are predicted, even when inertia is neglected. At large amplitude these oscillations are a description of experimentally observed stick slip and may be analogous to earthquake cycles. The character of spring block dynamics is largely governed by the relation of the spring stiffness K (stress per unit stretch) to a critical spring stiffness K_{crit} which is determined by the friction law. In the one state variable friction law used for the simulations presented here (where $d\tau_{ss}/dV|_{V_0} < 0$) K_{crit} is given by

$$K_{crit} = -\frac{1}{d_c}\frac{d\tau_{ss}}{d(\ln V)}\bigg|_{V_0} = \left(\frac{\sigma}{d_c}\right)\left(B - A + \frac{CV_t}{(V_0 + V_t)}\right) \tag{2a}$$

Spring Block and the Dimensionless Parameter $\mathcal{D}$

A common approach to understanding of slip stability is through comparison of an unloading frictional "stiffness" K_{crit} to an elastic stiffness K. This comparison, first done in the context of rate and state dependent friction by *Dieterich* [1979*a*], is facilitated by use of the dimensionless instability parameter $\mathcal{D}$:

$$\mathcal{D} \equiv K_{crit}/K \tag{2b}$$

One may regard $\mathcal{D}$ as a parameter to be varied from one simulation to another. A particularly simple set of simulations is that with constant driving speed. Steady block slip at constant speed (equal to the driving speed) is a possible motion for all values of $\mathcal{D}$. But small perturbations from this steady slip lead to three different behaviors depending on the value of $\mathcal{D}$. When $\mathcal{D} < 1$ ($K_{crit} < K$), a linearized analysis predicts that steady sliding is stable and that small (infinitesimal) perturbations decay back to steady sliding. If $\mathcal{D}$ is close to 1, this approach is oscillatory. When $\mathcal{D} = 1$ ($K_{crit} = K$), a linearized analysis predicts that steady sliding is neutrally stable and that small perturbations lead to constant amplitude oscillations. When $\mathcal{D} > 1$ ($K_{crit} > K$), a linearized analysis predicts that steady sliding is unstable and that small perturbations from steady sliding grow larger. This growth is oscillatory if $\mathcal{D}$ is close to 1.

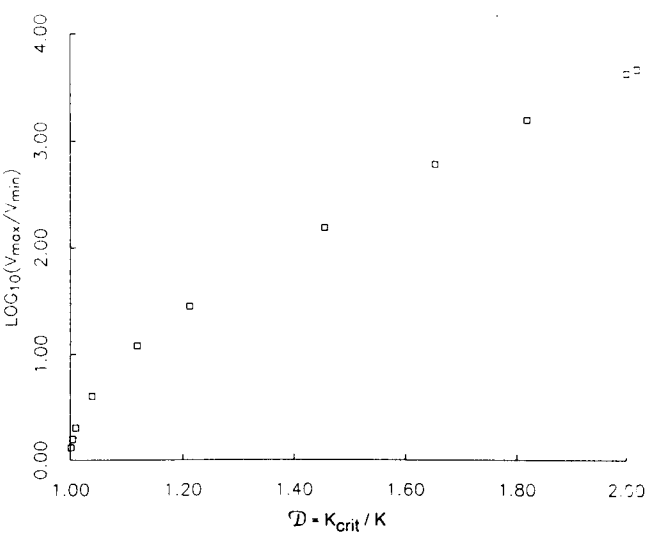

Fig. 3*a*. Results of spring block simulations using the friction law (equations (1) or (8a) and (8b)). Plotted is the range of velocity between fastest and slowest times during the limit cycle oscillation appropriate for the given stiffness parameter $\mathcal{D} = K_{crit}/K$. Note the strong dependence of amplitude on stiffness.

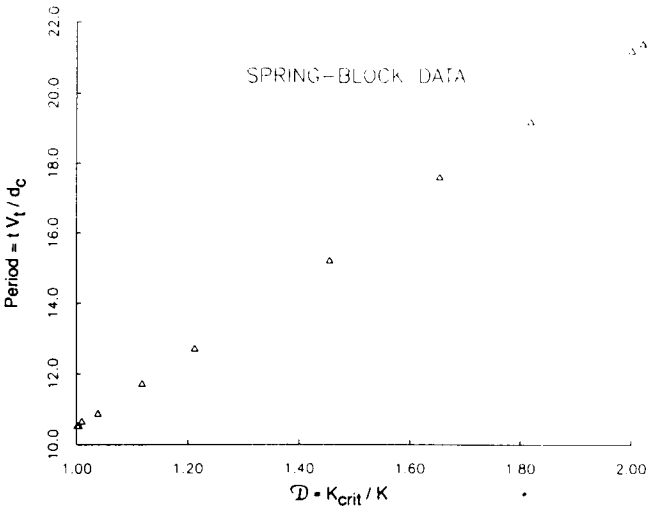

Fig. 3*b*. Oscillation period for the limit cycle motion (of Figure 3*a*) as a function of K_{crit}/K.

The behavior just described corresponds to a Hopf bifurcation at $\mathcal{D} = 1$ [*Gu et al.*, 1984]. In summary, large $\mathcal{D}$ ($\mathcal{D} > 1$) corresponds to instability, and small $\mathcal{D}$ ($\mathcal{D} < 1$) corresponds to stability, at least in a linearized analysis of steady sliding (see Appendix 1).

Using (1), with $C = 0$, *Gu et al.* [1984] have found analytic solutions for a massless spring block model in which finite amplitude periodic cycles exist at exactly $\mathcal{D} = 1$. These periodic motions are attained, say, by suddenly jumping the velocity of the loaded end of the spring during steady slip. Small jumps in the load point velocity lead to small oscillations, and larger jumps lead to larger oscillations. (Strictly, these periodic motions are not limit cycles since they are not unique in their neighborhoods.) For jumps of a critically large size, the resulting slip velocity becomes infinite in finite time. When $\mathcal{D}$ is less than 1, small perturbations from steady slip decay to steady slip, as predicted by the linearized analysis discussed above. But even when $\mathcal{D}$ is less than 1, sufficiently large perturbations were found to lead to infinite velocity in finite time. When $\mathcal{D}$ is greater than 1 perturbations of all sizes led to infinite velocities in finite time. For the particular friction law used by *Gu et al.* [1984], stable limit cycles never occur.

As previously discussed, the parameter values we use in (1) prevent the unbounded velocities found by *Gu et al.* [1984]. We find stable limit cycles in a spring block model using (1) for all (linearly unstable) values of $\mathcal{D}$ ($\mathcal{D} > 1$).

Figures 3*a* and 3*b* show the velocity range and period of these spring block limit cycles using the friction parameters given after (1) for a range of elastic stiffnesses. Figure 3*a* shows that when $\mathcal{D}$ is slightly above 1, the range of velocities observed is very small ($\log(V_{max}/V_{min})$ is close to zero). When $\mathcal{D}$ is much above 1, the velocity range is orders of magnitude larger. The amplitudes predicted here provide a rough lower bound on the velocity range in the spatially varying solutions presented later, where many effective spring constants, and hence $\mathcal{D}$ values, are active at once.

Although this is not a consequence of the particular friction law that we use, it is possible to construct a one state variable friction law which predicts limit cycles even when steady sliding is linearly stable. That is, it is possible to predict stick slip even when $d\tau_{ss}/dV \geq 0$ and steady sliding is stable. Also, using two state variables, *Horowitz* [1988*b*] has discussed some friction laws that predict the instability of steady slip even with $d\tau_{ss}/dV > 0$.

Other features of interest predicted by the spring block model and state variable friction laws include period doubling and (apparent) chaos (when two state variables are used in the friction law) [*Ruina*, 1983; *Gu et al.*, 1984].

SINE WAVE ELASTICITY SOLUTION

In our model the frictional surface is on the boundary of a deformable elastic solid. The friction equations can only be solved in conjunction with the relevant elasticity equations. We solve the elasticity equations using Fourier superposition of analytic solutions relating a sinusoidal shear traction on the slip surface to displacement on the slip surface.

The Stiffness Function $K(\kappa)$

All infinite planar fault models (with homogeneous-along-strike, linear-elastic surroundings) have the following property: sinusoidal shear traction on the fault causes an exactly out-of-phase (180°) sinusoidal tangential displacement via a (real-valued) effective spring constant K. This can be written as follows. If

$$\tau(x) = \sin(\kappa x - \phi) \tag{3a}$$

then

$$\delta(x) = -\frac{\tau(x)}{K(\kappa)} \tag{3b}$$

where τ is the shear traction on the fault, δ is the slip displacement, x is position along the fault, ϕ is the spatial phase shift, and the stiffness K depends on the wave number κ, geometry of the slab, and elastic constants [*Rice and Ruina*, 1983]. That sinusoidal shear stress and slip displacement are exactly out of phase for a large class of models follows from application of the elastic reciprocal theorem to two sinusoidal tractions with a phase difference of $\pi/2$ (J. Rice, personal communication, 1980).

Once one knows how a given traction distribution is composed as a sum of sine waves, the corresponding slip $\delta(x)$ is determined by a real superposition. The function $K(\kappa)$ (stiffness as a function of spatial frequency) fully characterizes the geometry and material effects of the elastic slab. The superposition of sine waves is equivalent to performing a Fourier transform on $\delta(x)$ (subtracting the boundary displacement), multiplying by $K(\kappa)$ to find the transform of τ and then performing an inverse transform to find $\tau(x)$, all of which is written

$$\tau(x) = -\frac{1}{2\pi}\int_{-\infty}^{+\infty} e^{-i\kappa x} K(\kappa) \left[\int_{-\infty}^{+\infty} e^{i\kappa x}\,(\delta(x) - V_0 t)\,dx\right] d\kappa \tag{3c}$$

Two-Dimensional Elastic Models

To determine $K(\kappa)$, one can use the solutions for a particular elastic model. Solutions for some two-dimensional elasticity (anti plane shear, plane stress, and plane strain) models are given in (4), (5), and (6) below.

Rice and Ruina [1983] give $K(\kappa)$ for an anti plane shear deformation (where one slab of Figure 1*b* goes into the plane of the figure, while the other one comes out) as

$$K(\kappa) = \frac{G|\kappa|}{2\tanh(|\kappa| H)} \quad \text{[anti plane shear]} \tag{4}$$

Marguerre [1931] presents the plane stress solution for a sinusoidal traction on the boundary of an elastic slab. After correcting some minor errors in his displacement function, $K(\kappa)$ can be found as

$$K(\kappa) = \frac{G|\kappa|\{T[Q_1 + (1-\nu)] - Q_1 - 4\}}{\{Q_1 T - T(3-\nu) - Q_1\}} \quad \text{[plane stress]} \tag{5}$$

where $G = E/2(1+\nu)$ is the shear modulus, $T \equiv \tanh(|\kappa|H)$, $Q_1 \equiv |\kappa|H(1+\nu)$, and ν is Poisson's ratio.

If the isotropic elastic law is expressed in terms of G and ν for plane stress, one can find a corresponding plane strain solution by substituting $\nu/(1-\nu)$ for ν in a plane stress solution. This substitution in (5) above gives $K(\kappa)$ for plane strain as

$$K(\kappa) = \frac{G|\kappa|\{T[Q_2 + (1-2\nu)/(1-\nu)] - Q_2 - 4\}}{\{Q_2 T - T(3-4\nu)/(1-\nu) - Q_2\}} \quad \text{[plane strain]} \tag{6}$$

where Q_2 is defined as $Q_2 \equiv |\kappa|H/(1-\nu)$ and T is defined as in (5).

One might find models (i.e., functions $K(\kappa)$) that take better account of the three dimensionality in Figure 1*a* than any of the two-dimensional models ((4), (5) and (6)). But in all cases, $K \approx G/2H$ when $\kappa = 0$ and increases monotonically with κ, becoming proportional to $G\kappa$ as $\kappa \to \infty$. Within these constraints we do not expect that the details of various elastic models have any effect on the variety of solutions predicted by the fault model. For example, plots of $K(\kappa)$ for anti plane shear (4) and for plane strain (6) with $\nu = 0$ are nearly identical (Figure 4*a*). In a few simulations

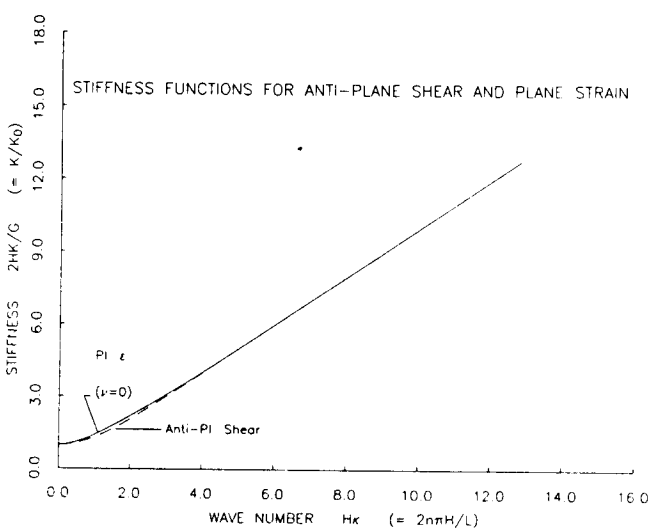

Fig. 4*a*. Stiffness $K(\kappa)$ as a function of wave number κ in the elasticity solution for a slab of thickness $2H$. The function is shown both for antiplane shear (4), that used in most of the simulations, and for plane strain (6) with $\nu = 0$.

(not shown here) we have compared fault slip motions based on plane strain solution (6) (with $\nu = 0$) to the anti plane shear solution (4). We observed only slight differences in the numerically calculated results and no difference in the qualitative nature of the solutions. Because of the simplicity of the analytic expression (4) as compared to (5) or (6), all solutions presented here are based on the anti plane shear $K(\kappa)$ (4).

Elastostatic Modes

As will be discussed later, we only consider slip that is spatially periodic with period L. Thus only discrete wave numbers κ_n appear in the Fourier superposition, and the Fourier transform is effectively a Fourier series. We define a stiffness K_n for a mode n by

$$K_n = K\left(\frac{2n\pi}{L}\right) \tag{7}$$

[e.g., $K_0 = K(0), K_3 = K(\frac{6\pi}{L})$]. Thus, for spatially periodic solutions the fault elasticity is fully characterized by the set of numbers K_n ($n = 0, 1, 2, ...$). The stiffness curves in Figure 4*b*, one for each n, show how K_n/K_0 depends on $L/H\pi$ for anti plane shear elasticity solutions (4).

Equivalence of Nonlocal Spring Block Model

Once the slip surface is discretized for numerical purposes, the elasticity could alternatively be defined by an appropriate set of springs connecting every node to every other node. Thus one may think of the surface points as interacting with each other in a nonlocal manner which is mediated by the two- (or three-) dimensional elastic material. Although our model is in this sense a spring block model we have paid attention to using a sufficient number of stiffly connected nodes that we accurately simulate an elastic continuum.

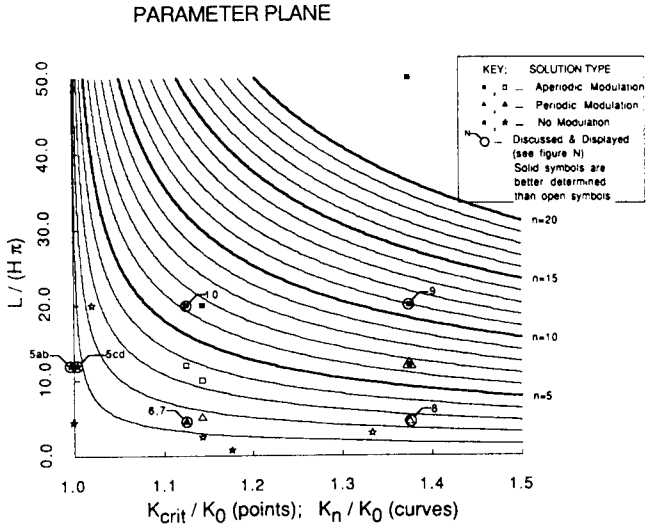

Fig. 4*b*. Elasticity and parameter plane. Curves show the elasticity relationship between nondimensionalized periodic length $L/(H\pi)$, a nondimensional stiffness K_n/K_0, and mode number n. Each curve corresponds to a single mode number n. These curves follow from the antiplane shear curves of Figure 4*a*. Plotted as points, using the same numerical values on the axis, are $L/H\pi$ and $\mathcal{D}$ for several model calculations. The shapes of the amplitude envelope modulations for simulations at the given parameter values are keyed in the box. The solutions displayed in subsequent figures are circled and labeled with their figure numbers. The relation of the elasticity curves to the parameter points is discussed in the text.

Inertia Is Neglected

Calculations are simplified considerably by neglecting inertia. The effect of elastodynamic radiation could be approximated by the addition of a linear viscous term to the friction law (1a). This viscous term, proposed by *Burridge and Knopoff* [1967], incorporates inertia exactly for an elastic half-space if its planar boundary does not deform. We have used such a linear viscous term in a few simulations (not shown here). Its effect, roughly like that of the C term in (1), is to damp large-amplitude motions.

Stability of Elastostatic Modes: K_n and K_{crit}

An important feature of the K_n is their relation to K_{crit}, where K_{crit} is the critical stiffness (2*a*) for unstable steady sliding in a linearized analysis. But, as with the single spring block, it is desirable to have one parameter to characterize the stability of the system. Since K_n increases with n, the greatest system instability is associated with K_0, and it is natural to use the parameter

$$\mathcal{D} \equiv K_{crit}/K_0$$

The values of two parameters $\mathcal{D}$ and $L/H\pi$, for the simulations presented here, are also plotted in Figure 4*b* as points (using the same numerical values on the axis for $\mathcal{D}$ as for K_n/K_0).

To find the approximate value of K_{crit}/K_n (the degree of instability for mode n in a given simulation), use Figure 4*b* as follows: read off $\mathcal{D}$ for that simulation, read off K_n/K_0 (from the nth curve) at the $L/H\pi$ value of the simulation, then find $K_{crit}/K_n = \mathcal{D}/(K_n/K_0)$. Values of K_{crit}/K_n greater than 1 mean that the nth mode is linearly unstable, while values less than 1 are linearly stable. This means that one finds the unstable modes visually from Figure 4*b* as those whose stiffness curves are to the left of the simulation point. The stable modes are those whose stiffness curves are to the right of the simulation point. For example, the solid square labeled with 10 inside a circle at $L/(H\pi) = 20$ and $\mathcal{D} = 1.125$ has seven linearly unstable modes. The K_{crit}/K_n ratios for simulation 10 are $K_{crit}/K_0 = 1.125$, $K_{crit}/K_1 = 1.120$, $K_{crit}/K_2 = 1.109$, ..., $K_{crit}/K_6 = 1.005$, $K_{crit}/K_7 = 0.967$, etc.

Discussion of Governing Equations

Here we summarize the governing equations in a nondimensional form; they are

$$\hat{\tau} = \hat{\theta} + \ln(\hat{V}) \tag{8a}$$

$$\dot{\hat{\theta}} = -\hat{V}\left[\hat{\theta} + \hat{B}\ln\left(\hat{V}\right) + \hat{C}\ln\left(\frac{\hat{V}}{1+\hat{V}}\right)\right] \tag{8b}$$

$$\dot{\hat{\tau}} = -\frac{1}{2\pi}\int_{-\infty}^{+\infty} e^{-ik\hat{x}}\hat{K}(\hat{\kappa})\left[\int_{-\infty}^{+\infty} e^{ik\hat{x}}\left(\hat{V} - \hat{V}_0\right) d\hat{x}\right] d\hat{\kappa} \tag{8c}$$

with $\hat{K}(\hat{\kappa}) = \hat{K}_0|\hat{\kappa}|/tanh|\hat{\kappa}|$. Equations (8*a*) and (8*b*) are the friction law from (1*a*) and (1*b*). Equation (8*c*) is the time

derivative of (3c), the relation between slip displacement and shear traction as governed by the elasticity equations.

The dependent variables $\hat{\tau} = (\tau/(\sigma A) - \mu_0/A)$, $\hat{\theta} = \theta/A$, and $\hat{V} = V/V_t$ are functions of the independent variables $\hat{t} = V_t t/d_c$ and $\hat{x} = x/H$. The quantity $\hat{\kappa} = H\kappa$ is a dummy transform variable. Parameters (with the values that we used in the simulations) are $\hat{V}_0 = V_0/V_t = 1$, $\hat{B} = B/A = 0.909$, $\hat{C} = C/A = 0.909$, and $\hat{K}_0 = Gd_c/(2\sigma AH)$, which was varied.

It should be noted [*Tse and Rice*, 1986] that since μ_0 does not appear in the governing equations (8), the predicted motions are independent of the background friction coefficient. Thus the solutions found here apply equally to "high stress" and "low stress" faults.

Symmetry of Governing Equations

The governing equations have symmetries that should be noted for two reasons. First of all, the extent to which the solutions have the same symmetries as the governing equations is interesting. Second, every solution of the governing equations is related to a family of solutions through the symmetries of the governing equations.

The model is spatially homogeneous and has no explicit dependence on time so the equations are invariant to time and space translation. That is, replacing $(\hat{x}, \hat{t})$ with $(\hat{x} - \hat{x}_0, \hat{t} - \hat{t}_0)$, where $\hat{x}_0$ and $\hat{t}_0$ are any real constants, does not alter the governing equations. So any solution generates a family of solutions by replacing $(\hat{x}, \hat{t})$ with $(\hat{x} - \hat{x}_0, \hat{t} - \hat{t}_0)$, where $\hat{x}_0$ and $\hat{t}_0$ parameterize the family. For reasons that one can infer by looking at Figure 1b from the front and back of the page, the equations are also invariant to reflection in space. That is $-\hat{x}$ can be substituted for $\hat{x}$ without altering the equations, and a solution reflected in space is a new solution.

Periodic Boundary Conditions

Numerical solution forces the use of a finite spatial domain for the fault. In order to eliminate end effects we have used periodic boundary conditions, with period L. In the region over which we solve, the leftmost and rightmost points are tied together exactly as any other neighboring points anywhere else on the fault. Periodic solutions are still solutions to the original infinite problem, but there are presumably spatially nonperiodic solutions to the infinite problem that cannot be found with the periodic restriction. Also, solutions to the infinite problem found using the periodic constraint might change their character in time if subject to small perturbations and no periodic constraint.

The periodic boundary condition reduces the Fourier transform of (8c) to a Fourier series. The continuous transform variable $\hat{\kappa}$ is replaced with the sequence of wave numbers $\hat{\kappa}_n \equiv 2n(\pi H/L)$. The important translation (in space and time) and reflection (in space) invariance of the original equations is preserved by the periodic boundary condition.

The periodic boundary condition may be regarded as a simplification that allows us to do a finite domain problem with relatively little difficulty, or an artifact that the numerical method imposes on our infinite problem. For better or worse, L (or the dimensionless ratio $L/H\pi$) is a parameter that affects the solutions. One expects that for large $L/H\pi$ the qualitative features of the solutions are not distinguishable from the infinite problem, $L/H\pi \rightarrow \infty$.

Parameters Varied in the Calculations

The remainder of this paper discusses solutions of (8) with periodic boundary conditions. The two parameters that we systematically vary are $\hat{K}_0$ (equivalent to varying any of d_c, σ, G, H, or a proportional change in all of A, B, and C) and $L/H\pi$.

Instead of reporting the value of $\hat{K}_0$ in our discussion we report the value of the dimensionless stability parameter $\mathcal{D}$ which we have generalized from (2b) as $\mathcal{D} \equiv K_{crit}/K_0$.

$$\mathcal{D} \equiv \frac{\hat{K}_{crit}}{\hat{K}_0} = \frac{-\left(1 - \hat{B} - \hat{C} + \hat{C}\hat{V}_0/(1 + \hat{V}_0)\right)}{\hat{K}_0} \qquad (9a)$$

$$\mathcal{D} = \frac{K_{crit}}{K_0} = -\frac{2\sigma H}{Gd_c}\left(A - B - C + \frac{CV_0}{V_t + V_0}\right) \qquad (9b)$$

Characteristic Lengths

Equation (9b) shows that the instability parameter $\mathcal{D}$ can also be viewed as proportional to the ratio of a characteristic length in the elastic solid H to a characteristic length found from the friction law and the elastic constants (all terms besides H in (9b)). In very rough terms one might think of this latter length as the size of a breakdown zone in a shear fracture model [*Tse and Rice*, 1986].

SOLUTIONS TO THE LINEARIZED EQUATIONS

Before proceeding to the numerical solutions of the nonlinear continuum problem we first discuss what is known or might be surmised about them from a linearized continuum analysis.

In the problem considered here, steady slip at the driving rate is a solution of the governing equations (i.e., $V(x,t) \equiv V_0$, $\dot{\theta}(x,t) \equiv 0$). One can consider small perturbations to this solution. The linearized analysis of *Rice and Ruina* [1983] is then applicable. In the linearized solutions, spatial perturbations can again be constructed from a sum of sine wave perturbations each with wave number κ. But unlike the nonlinear problem that we consider here, in the linear problem each wavelength perturbation grows or dies in time independently of other wavelengths. Each wavelength perturbation behaves exactly like a spring block model with the appropriate stiffness $K(\kappa)$. If the slab is compliant enough, there is a critical wave number κ_{crit} which has the associated stiffness $K_{crit} \equiv K(\kappa_{crit})$. All waves of perturbation from steady sliding with smaller wave number than this critical wave (greater wavelength) grow exponentially in time. The longer the wavelength, the faster the exponential growth. Waves with wave number greater than κ_{crit} (smaller wavelength) decay toward zero amplitude. Perturbations with the critical wave number $\kappa = \kappa_{crit}$ persist. They manifest themselves as oscillating standing waves of arbitrary (in both space and time) phase. Superposition of two such waves of appropriate relative phase leads to propagating creep waves. Both right going and left going creep waves are solutions. The work presented here was in fact originally motivated by a desire to find a nonlinear generalization of these creep wave solutions.

In the linearized solutions, longer-wavelength perturbations grow exponentially faster than shorter-wavelength perturbations. So a random initial condition, which contains all wavelengths, will lead to solutions which are eventually dom-

inated by homogeneous (κ=0, wavelength=∞, or mode 0) slip motion. This property of the linear solution might suggest that eventually all motions in our nonlinear model will reduce to homogeneous motions, with all points on the fault moving in unison. This is not what we observe, however, in the numerical simulations described below.

NONLINEAR SINGLE SRING BLOCK SOLUTIONS TO THE CONTINUUM MODEL

The nonlinear spring block solutions discussed previously are directly relevant to the elastic slab model since spring block solutions are solutions to the elastic slab equations (8). However, they are only precisely applicable when the initial conditions are spatially homogeneous.

One can also use the single spring block solutions to speculate about the behavior or the continuum problem for nonhomogeneous initial conditions. From the exponential growth in the linearized continuum solutions we were led to the tentative guess that spatially homogeneous motion (mode 0) would eventually dominate the motion for any initial conditions. But a contrasting guess can be constructed from the nonlinear oscillatory spring block solutions. One might imagine that each spatial mode behaves as a single spring block and is decoupled from every other mode. The fault motion thus predicted is a sum of spatial sinelike waves of various wavelengths each oscillating at its own frequency (in a possibly nonsinusoidal manner). The resulting motion would appear complicated in space-time though spikes in the Fourier transform in time (or space-time) would reveal its underlying simplicity.

NUMERICAL METHOD

The details and general principles involved in our time stepping numerical solution are explained in Appendix 2.

Node Spacing and the Continuum Approximation

We assume that the continuum equations (8) have solutions that are smooth (have no discontinuities in value and slope) and demand that the numerical solutions should show this smoothness. A criterion for achieving this smoothness is that node spacing be close enough so that all computed variables (e.g., stress and slip rate) and their spatial derivatives (as calculated with first differences) vary much less from one node to another than their total variation over all nodes.

We have not found a formula for choosing an adequately close nodal spacing to meet this criterion. Clearly, a necessary criterion is that the nodal spacing be such that $K_{N/2} > K_{crit}$ (i.e., that the stiffness associated with motion between neighboring nodes be greater than the critical stiffness) since otherwise one node could exhibit spring block dynamics out of step with the motions of its immediate neighbor. Thus *Tse and Rice* [1986] claimed that if the characteristic length in the friction law d_c is reduced from one simulation to the next, then accurate continuum modeling requires that node spacing be proportionally reduced. For a fixed physical model this corresponds to proportionally increasing the number of nodes with $1/d_c$, so as to keep $K_{N/2} > K_{crit}$ (since K_{crit} is proportional to $1/d_c$ and $K_{N/2}$ is proportional to N). *Tse and Rice* [1986] also present a fracture mechanics argument that the size of a breakdown zone would scale with the distance d_c for equilibrium crack growth and a rate-independent friction law. We have found from our numerical solutions that nodal space scaling based on the arguments above are not adequate. More nodes are required to smoothly represent the shear fracture or dislocationlike stress concentrations that arise in the simulations, perhaps because the effective stress drop in the propagating events ($\approx$fractures) is also a function of d_c. The node closeness required for relatively small node-to-node variation in the values of variables was found to be a very strongly increasing function of $\mathcal{D} = K_{crit}/K_0$, going from 32 to 1024 when $\mathcal{D}$ changed from 1.1 to 1.6 for a fixed $L/H\pi$. The numerical results that we show do have small node-to-node variations and thus seem to properly capture the continuum ($N \to \infty$) solutions.

The time steps, adjusted as described in Appendix 2, also decrease in size with increased $\mathcal{D}$, since slip events then involve faster slip rates and greater accelerations.

NUMERICAL SOLUTIONS

The numerically predicted stress and motion ($\tau(x,t)$, $V(x,t)$) depend on model parameter values and initial conditions. The parameters varied in the simulations here are $\mathcal{D} \equiv K_{crit}/K_0$ (keeping $\hat{B}$ and $\hat{C}$ constant) and $L/H\pi$, the axes for the points in Figure 4*b*. Initial conditions were either those that we thought might generate steady propagating creep waves or small random perturbations from steady sliding. Solutions were continued in time until the long-term nature of the solution was determined or until cost concerns intervened. The qualitative nature of the solution at long times was only once seen to depend on initial conditions. The two points on Figure 4*b* halfway between the numbered points (8 and 9) have different solution types following from two different initial conditions. Evidently, for some parameter values the phase space of our solutions seems to have more than one region of attraction.

Small-Amplitude Nearly Spring Block Motion

Simple, nearly spring block, fault motion is shown in Figures 5*a*–5*d* for fault motion very near $\mathcal{D} = 1$. Wherever $\mathcal{D}$ is less than 1, we find the fault asymptotically tends toward a stable solution of steady sliding at the far-field driving velocity V_0. This is exemplified by the simulations labeled with a circled star as "5ab" just to the left of the $L/H\pi$ axis at $L/H\pi = 12$ on the parameter plane of Figure 4*b*. Figure 5*a* shows the time history of the slip velocity at a particular point along the fault when $\mathcal{D}$ is just less than 1. In Figure 5*a*, the slip rate is oscillating at one node with the amplitude of oscillation decaying approximately exponentially in time toward the ultimate steady sliding solution. For simulations using other parameters (below) the amplitude envelopes of such one node traces show different shapes. Figure 5*b* shows the ultimate spatially homogeneous slip from the solution in Figure 5*a*. Slip is displayed as a function of position along the fault at a sequence of times. Slip displacement monotonically increases in time (no back slip) in all of our simulations. Hence the sequence of displacement curves never cross each other. In similar figures below, the time intervals between curves may vary as slip progresses allowing the shape of the slip distribution to be seen during both rapid and slow slip.

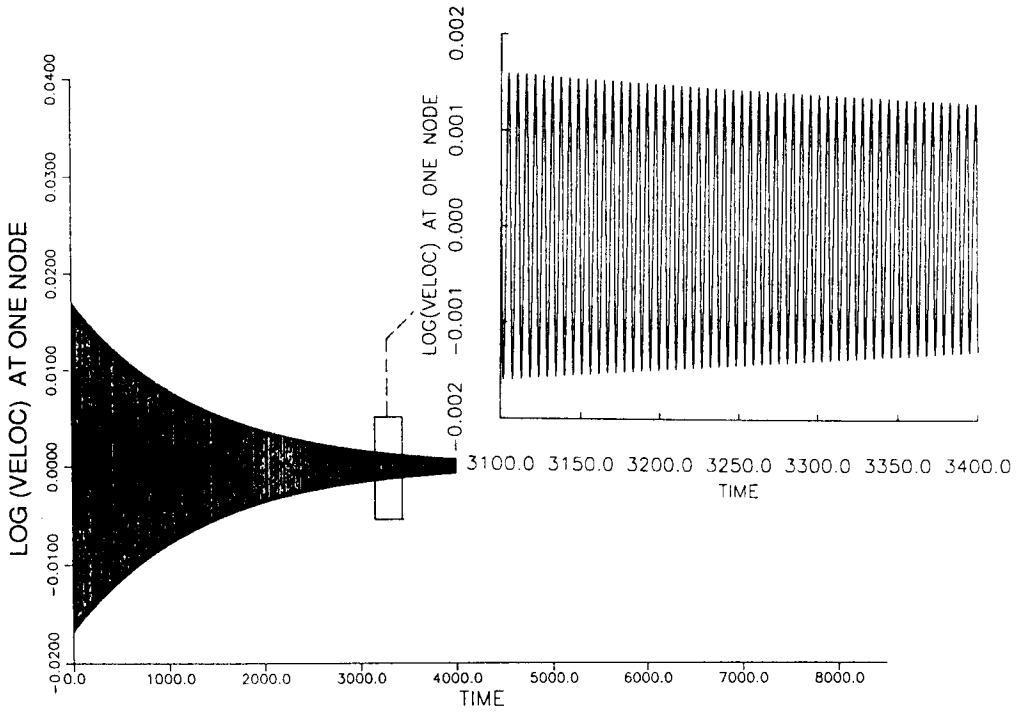

Fig. 5*a*. Solutions near the mode 0 oscillation boundary. $L/H\pi = 12.0$, $\mathcal{D} = K_{crit}/K_0 \approx 1$. Amplitude envelope for a one node trace at $\mathcal{D} = 0.99$ showing velocity oscillations decaying with time. Many oscillations are compressed together in order to show the shape of the amplitude envelope.

When $\mathcal{D}$ is slightly over 1 (Figures 5*c* and 5*d*), we find the entire fault executing sustained "spring block" ($\kappa = 0$) oscillations. Figure 5*c* displays friction stress as a function of time and position for very small, nearly homogeneous oscillations. The surface plot and the contour plot underneath present the same results two different ways. A slight amount of nonhomogeneous spatial structure is found in this solution, visible as a closed narrow contour in Figure 5*c* and is a remnant of a heterogeneous initial condition.

Amplitude Envelopes

The above solutions all lead to a constant amplitude envelope in a long time plot of slip velocity at one node versus time. With other parameter values we find other shapes for the amplitude envelope. We have catalogued our solutions by the shape of these amplitude envelopes in the legend of Figure 4*b* as constant (no modulation), periodic, or aperiodic. A constant amplitude envelope corresponds

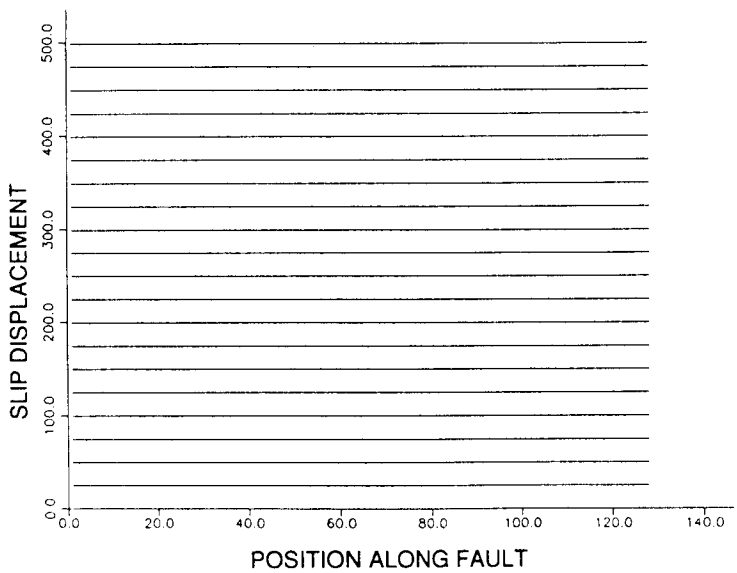

Fig. 5*b*. Slip displacement versus position at a sequence of times showing spatial mode 0 deformation at an essentially constant slip rate. $\mathcal{D} = 0.99$.

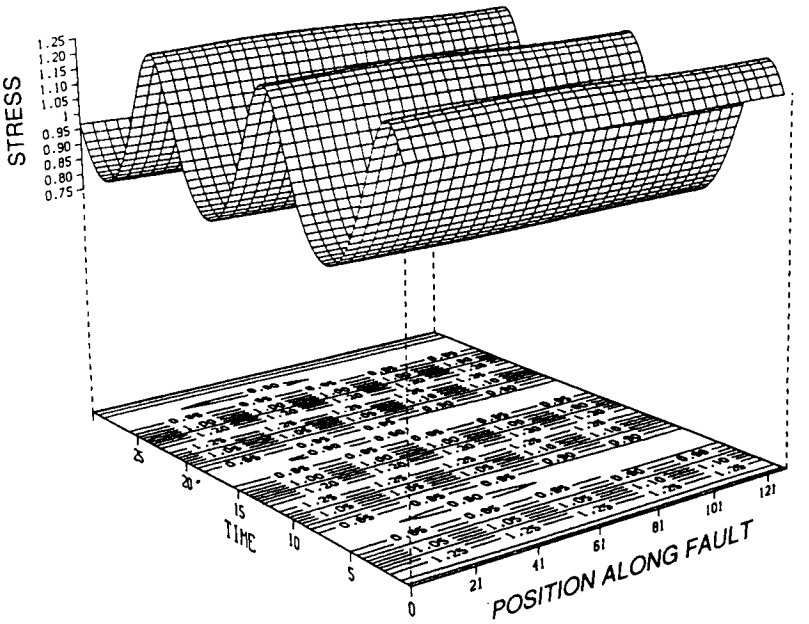

Fig. 5c. Perspective plot showing small amplitude mode 0 oscillations. $\mathcal{D} = 1.01$.

to a periodic solution of the governing equations. A periodically modulated amplitude envelope corresponds to a quasi-periodic (or possibly periodic with a longer period) solution. And an apparently aperiodic amplitude envelope corresponds to a chaotic (or possibly quasi-periodic with multiple period) solution.

Mode 0 Solutions

If the initial condition is pure mode 0 (spatially homogeneous), then the linearized theory of *Rice and Ruina* [1983] predicts a pure mode 0 solution for all time. Symmetry requires that in our nonlinear problem, no matter how large $\mathcal{D}$ is, we will also obtain a spatially homogeneous solution. But numerical simulations indicate that for $\mathcal{D}$ somewhat greater than 1 spatial homogeneity in the oscillatory mode 0 motion is unstable with respect to small spatial perturbations.

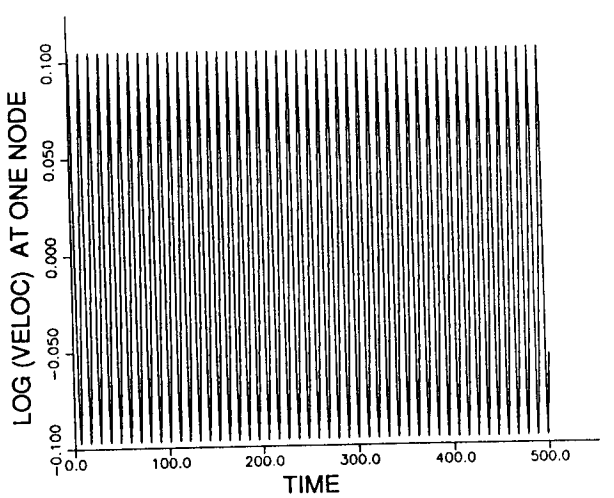

Fig. 5d. One node trace for $\mathcal{D} = 1.01$ showing velocity oscillations maintained with time.

That is, if a little bit of spatial noise is added to the initial conditions, or even if one node is perturbed, the solution will evolve into a nonhomogeneous solution of a type depending on its parameter values.

Standing Waves and Traveling Waves

We know of two persistent solutions to the linearized equations of our model: standing waves and traveling waves. The homogeneous (mode 0) oscillations described above are examples of standing waves. Both standing waves and creep waves seem to have corresponding fully nonlinear solutions. These special solutions seem to require precise initial conditions.

A mode 1 creep wave solution is shown in Figure 6. This solution was found by performing a sequence of simulations. An analytically constructed linearized creep-wave of *Rice and Ruina* [1983] was used as an initial condition for a numerical nonlinear simulation with nonphysical $K(\kappa)$ values ($K(\kappa = \kappa_{wave}) < K_{crit}$ and $K(\kappa < \kappa_{wave}) > K_{crit}$) which let the wave grow in size without substantially changing shape. A wave grown in this manner was then used as an initial condition for the model with $K(\kappa)$ like those in the other simulations presented here (where K increases with κ). When properly started, the wave will traverse the length of the fault many times. However, in all of our continuum simulations with sufficiently large N, the creep wave transforms to another solution type after a large number of cycles. Using just eight nodes, we once did obtain a steady creep wave, but with an increase in the number of nodes (and the quality of the continuum approximation) the wave changed shape. We think that creep waves are a solution of the continuum system but are unstable to slight perturbations.

Though steady creep waves are interesting in their own right, they may not be of much geophysical significance since they require precise initial conditions and eventually change their form if there is even slight deviation from these conditions.

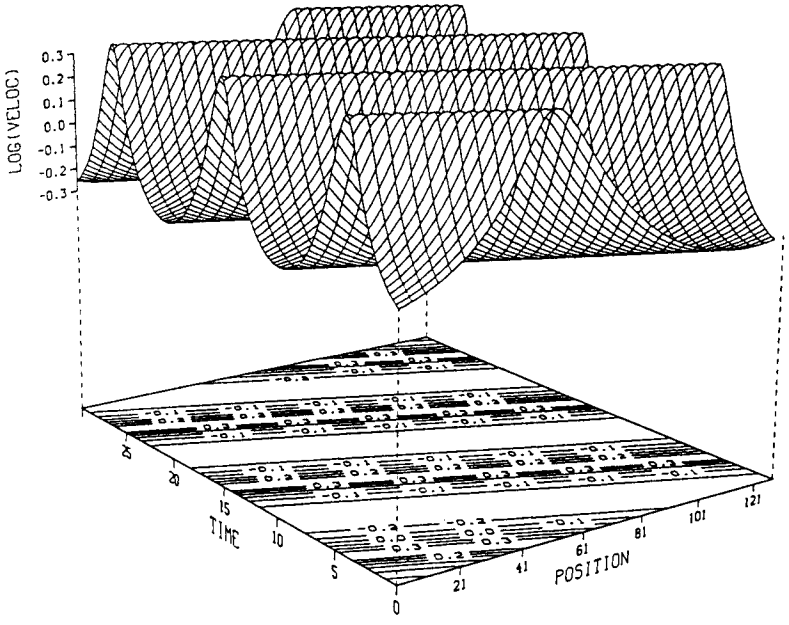

Fig. 6. Creep wave. $L/H\pi = 4.5$, $\mathcal{D} = 1.125$. One of the special solutions possibly existing anywhere on the parameter plane. After some time this motion changed into the motion shown in Figure 7.

Periodic Amplitude Envelopes

In contrast to the solutions just discussed we have found motions which seem stable in that they seem to maintain their qualitative nature forever. A relatively simple example of such a solution is shown in Figures 7*a*–7*c* (note the difference in time scale between Figure 7*a* and Figures 7*b* and 7*c*). The solution changes shape slightly from cycle to cycle. Over the span of about 100 cycles, the region of fastest slip moves from one point on the fault (Figure 7*b*) to another (Figure 7*c*) and back again. Thus the slip velocity amplitude envelope is periodic with a period of about 100 spring-block-like cycles (Figure 7*a*). The unstable creep wave of Figure 6 is also from this point in the parameter plane.

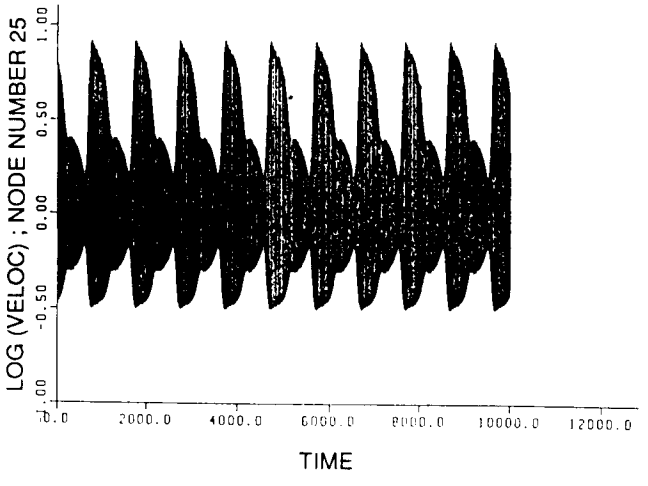

Fig. 7*a*. Periodic amplitude envelope for velocity versus time at one node. The period is about 1000 time units. The solution has the simple spatial structure shown in Figures 7*b* and 7*c*. $L/H\pi = 4.5$, $\mathcal{D} = 1.125$.

Steadily Drifting Event Center

Figures 8*a*–8*c* show another relatively simple solution with a periodic amplitude envelope. However, in contrast with Figures 7, the solution of Figures 8 shows an event that moves leftward from cycle to cycle. This displacement, combined with the periodic boundary conditions (by which the extension of the fault to the left is the right end of the fault), leads to the periodic amplitude envelope observed in Figure 8*c*. The combination results in a solution that is periodic in space-time (i.e., $f(x,t) = f(x + x_0, t + t_0)$, where x_0 and t_0 are constant and (x_0, t_0) is the period in space-time). This space-time periodicity is another example of a type of evolution found in this system. Note that the plot in Figure 8*c* is not exactly periodic (e.g., the details of the three small time scale spikes are different in the two amplitude envelope peaks) since the drift per cycle is not an integer fraction of the fault length. Thus the solution is quasi-periodic in time.

Complex Events

Figure 9 shows an example of a complex global event. This type of solution has the whole fault moving quickly at about the same point in time but with strong events at several different positions and slightly different times. The amplitude envelope of Figure 9*c* is apparently aperiodic. This solution evolves in an irregular way. The patterns of shading in the long-duration serial plot of Figure 9*a*, show the loci of strong events changing with time. It must be reemphasized, however, that our simulations are on a spatially homogeneous fault. No strong or weak patches are built into the material properties along the fault, and hence event centers occur where they do only because of the fault's prior history.

Figure 10 shows another complex simulation. Motion at a given point is still a modulated oscillation, but the shape and amplitude of the oscillation vary from point to point. In the time period of Figure 10*a*, node 12 moves at nearly a constant rate. Near the start time of Figure 10*a* a creep-like

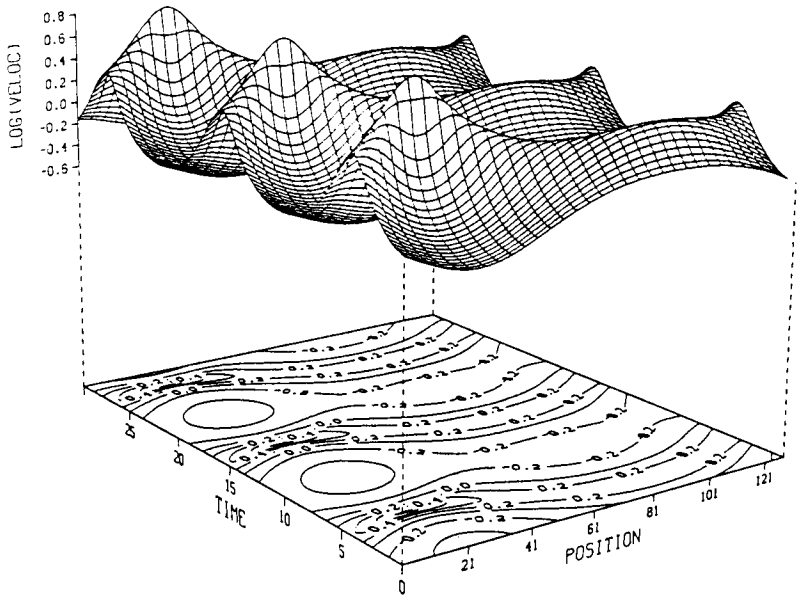

Fig. 7*b*. Perspective view of the solution of Figure 7*a* during one part of the amplitude modulation.

event propagates from node 60 to node 40 where fast slip is then triggered. Like the solution of Figure 9, the shape of this solution also slowly changes over many cycles leading to the apparently aperiodic amplitude envelope in Figure 10*b*. From Figure 10*a* the velocity fluctuates over roughly 1.2–1.4 orders of magnitude. This is slightly greater than the rough lower bound of 1 order of magnitude provided by the single spring block velocity range data of Figure 3*a*. Complex solutions of this type have been found only at high values of $L/H\pi$.

DISCUSSION

Number of Active Spatial Modes

The dependence of solution type on parameter values is summarized by the key labeling the points on the parameter plane of Figure 4*b*. The relation of a given point to the stiffness of the various mode numbers determines the number of spatially sinusoidal modes that are linearly unstable for the given parameter values.

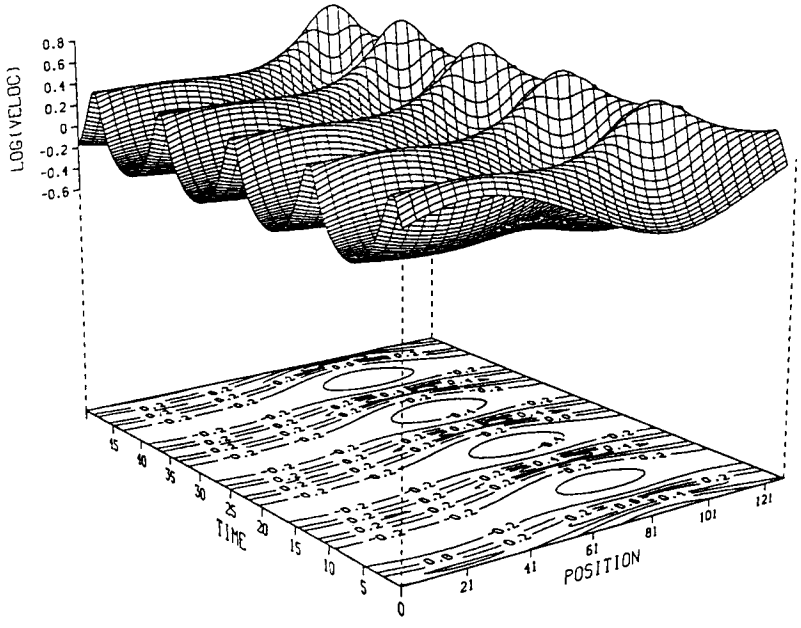

Fig. 7*c* The solution of Figure 7*a* at another part of the amplitude envelope. Over the course of one amplitude envelope cycle the solution changes from that shown in Figure 7*b* to that in Figure 7*c* and back.

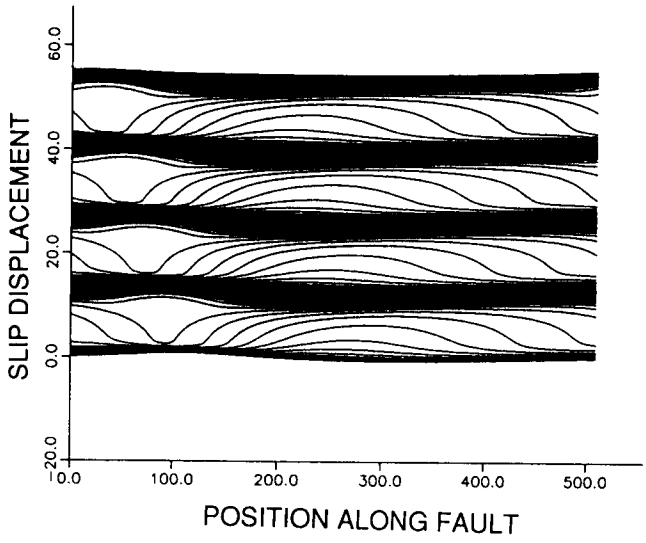

Fig. 8a. Simple spatial structure, periodic in space-time. $L/H\pi = 4.5$, $\mathcal{D} = 1.375$. Slip displacement versus position at a sequence of times is shown. One simple event center (region of high-speed slip) drifts from cycle to cycle with a constant speed. The whole fault is quiet for a long time (dark black bands) until faster motion begins. Two "creep wave"-like events spread out (with different propagation velocities) from a nucleation site (initially at about node 250 or so). Where they meet, the high-velocity event occurs. The time interval between individual lines is constant (but not an integer fraction of the period of the cycle.)

At a typical instant in time, long after transients from the initial conditions have washed out, the fully nonlinear solutions have about the same number of spatial maxima or minima in velocity or slip displacement as they have linearly unstable modes. For the simulations reported here, Figure 7 has one maximum and modes 0 and 1 linearly unstable; Figure 8 also has one maximum but modes 0, 1, and 2 unstable; Figure 9 has about eight maxima and modes 0–11 unstable; and Figure 10 has about five maxima and modes 0–6 unstable. So it appears that all linearly unstable modes (wavelengths) are active (have nonnegligible Fourier components) in the general solution of this problem.

Continuing our earlier speculations based on single spring block solutions, perhaps the strength of a spatial mode's activity may be correlated with K_{crit}/K_n for that mode (see Figure 3). Modes with a large K_{crit}/K_n ratio (very unstable) seem to appear with larger amplitudes than modes with a small ratio (slightly unstable). This would be predicted if spatial modes behaved as fully uncoupled single spring blocks. If many spatial modes had roughly equal degree of linear instability, then they would have roughly equal spectral components in the nonlinear solution. Figure 4*b* shows that at high values of $L/H\pi$, many low wave number (long wavelength) modes have K_{crit}/K_n values nearly equal to $\mathcal{D}$. Thus, if the spatial structure is in fact reasonably well described by the linearly unstable modes, these low wave number modes would appear in solutions with amplitudes approximately equal to that of mode 0. On the other hand, the solutions shown in Figures 7, 8, and 9 clearly indicate coupling between modes since all parts of the fault move in a nearly coordinated motion. However, a possible explanation of Figure 10 is that the competition (beating) between nearly independent modes results in the visual complexity observed.

Large Values of $\mathcal{D}$

A friction law in which friction depends on the instantaneous rate of slip is obtained by the singular limit $d_c \to 0$ in which case $\tau \equiv \tau_{ss}$, and τ is governed entirely by (1c).

As expected from spring block simulations, we find that as $\mathcal{D}$ increases, the magnitude of velocity peaks increases (for

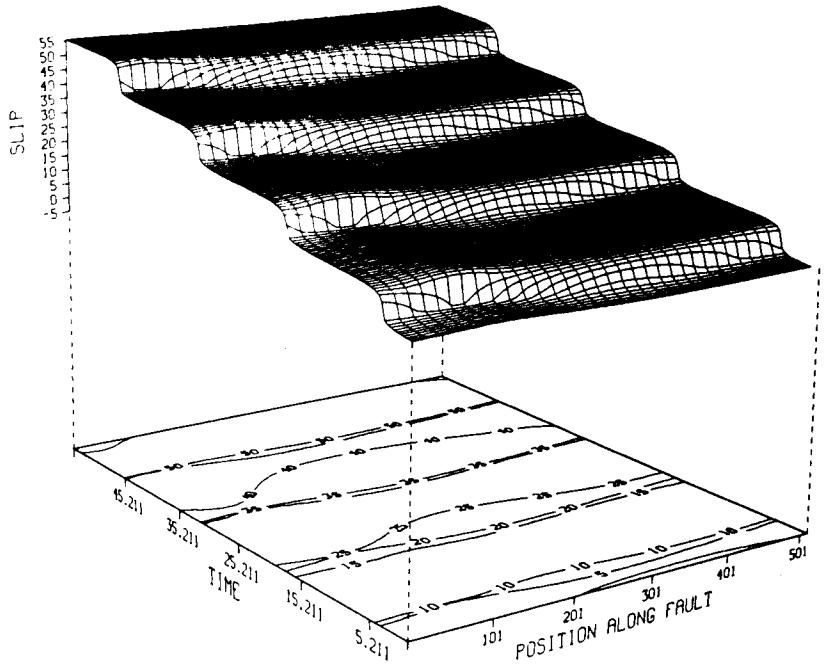

Fig. 8b. A perspective plot of the events of Figure 8a. The fault is quiet (although slowly slipping) for long times between moments of activity.

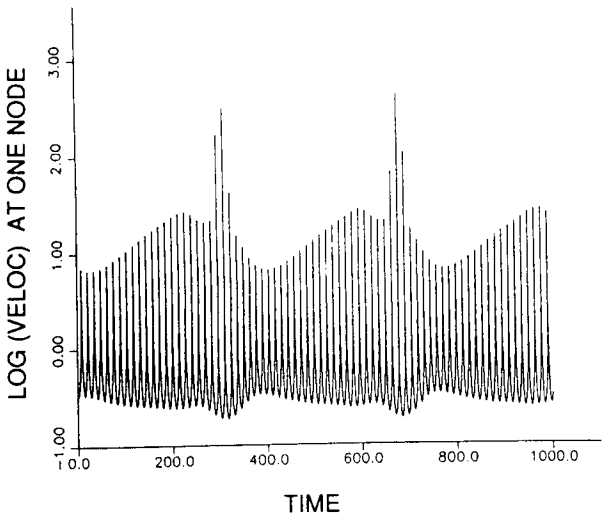

Fig. 8c. Velocity at node 25 is plotted for 62 cycles of the motion shown in Figures 8a and 8b. The periodic modulation of the amplitude envelope is caused by the event center moving past node 25. Note that the velocity range for the event center (high peaks) is about 1 order of magnitude higher than for the rest of the fault.

all initial conditions). Seismic emissions (nodal velocities reaching very high values) would occur in this model if $\mathcal{D}$ were high enough. For high $\mathcal{D}$ an accurate model clearly would require the inclusion of inertia (neglected here).

Additionally, as $\mathcal{D}$ increases, the spatial gradient of velocity increases in the region between quickly slipping and slowly slipping regions on the fault. The effect of $\mathcal{D}$ on both velocity gradients and peak magnitudes requires a great increase the number of nodes in order to provide an appropriately smooth solution. Thus $\mathcal{D}$ strongly affects the cost of computation. Computation time goes from minutes to hours with a change in $\mathcal{D}$ from 1.1 to 1.5.

The parameter values used in our simulations were not chosen for their geophysical significance. Accurate geophysical modeling may require much greater values for $\mathcal{D}$ than used in any of the simulations here. For some purposes, $\mathcal{D} \equiv K_{crit}/K_0$ is reasonably approximated by $\hat{K}_0^{-1} = \sigma HA/(Gd_c)$, the value it would have if we had used $C = 0$ and $B = 2A$ in the friction law. It is the (possibly) large ratio of plate thickness H to friction transient length d_c that, compared to σ/G, drives $\mathcal{D}$ to (possibly) large values. Once we have assumed that B is greater than A (so $d\tau_{ss}/dV < 0$), it is the indeterminacy of the length d_c that seems to be of greatest importance in determining the qualitative na-

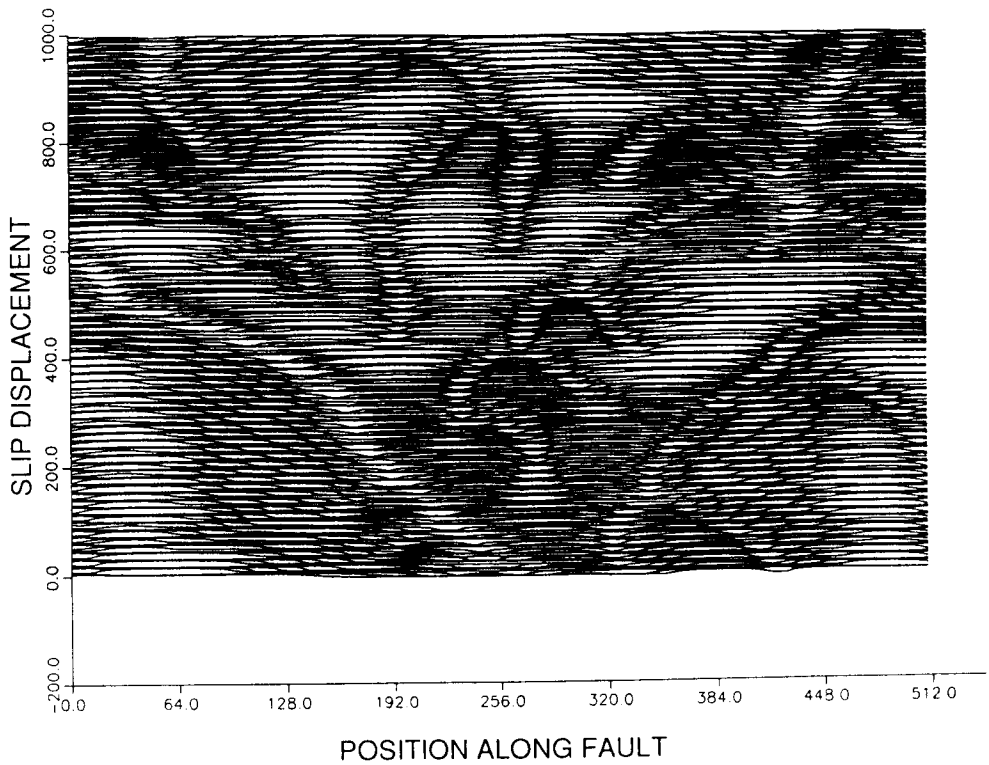

Fig. 9a. Complex global event. $L/H\pi = 20.0$, $\mathcal{D} = 1.375$. Slip displacement versus position is shown for a large number of times. At a given point on the fault repeated slip, with a period about equal to that for a spring block with the same $\mathcal{D}$ (= 1.375), is followed by near quiescence. The details of the slip distribution only change slightly in each cycle so the motion appears nearly periodic over a time period of a few cycles. But the details of the slip distribution change drastically over many cycles. Many event centers (regions of high slip speed) are active during the same overall cycle. Event centers are visible as light colored regions (high slip speed gives sparse line spacing and light color) surrounded by darker regions with (barely visible) converging "creep waves" (see Figure 8b for clear examples of "event centers" and "creep waves"). The wider light regions are "creep wave" nucleation sites. The long-term evolution of the solution is complex. Notice that event centers migrate different amounts from event to event, are created where none previously existed, become inactive, and merge with others over the duration of this figure.

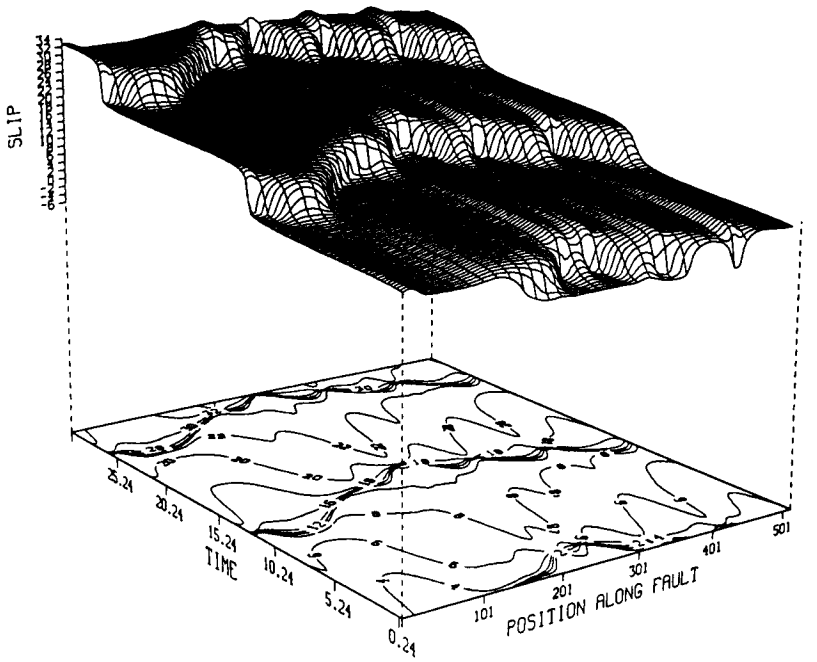

Fig. 9b. A perspective view of the first few cycles of Figure 9a. The character is similar to Figure 8 in that there are long times of relative quiet followed by periods of activity. Close examination reveals a change of the activity patterns in just these three cycles: the two events centered around node 250 or so in the first cycle merge into a broad single event at the second cycle that becomes narrower at the third cycle.

ture of the solution. In the extreme one might let $d_c \to 0$, thus replacing the state variable friction law with a instantaneous velocity-dependent friction law. This is equivalent to $\mathcal{D} \to \infty$, however, and the nature of solutions at this extreme is unstudied. One would hope for an asymptotic theory to supersede the full calculations in that case. On the other hand, it is possible that high values of $\mathcal{D}$ affect the dynamics of fault systems as strongly as high values of the Reynolds number affects the dynamics of fluid flow. Thus understanding the dynamics of high $\mathcal{D}$ fault slip may be as difficult a problem as understanding high Reynolds number (turbulent) fluid flow. The geophysical importance of these problems depends on the size of a field relevant value for d_c.

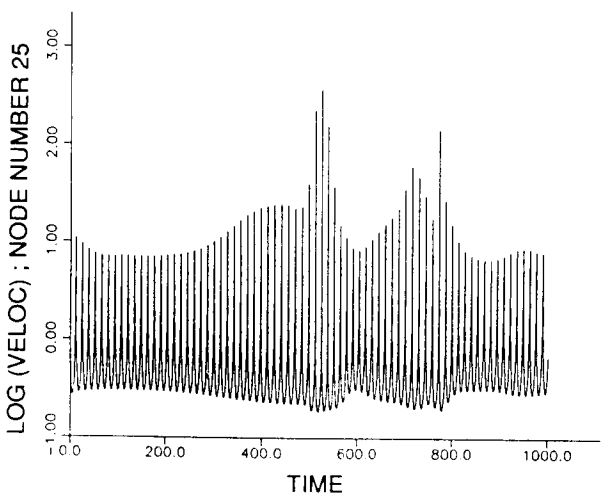

Fig. 9c. The aperiodic amplitude envelope slip velocity versus time at node 25 for the duration of Figure 9a. The high-speed peaks at around 550 and 780 time units represent an event center migrating past node 25. The velocity range for these event centers is about 2 orders of magnitude higher than the surrounding fault.

Implications for Prediction

This model, as well as any other model which is expressed as a system of differential equations, is inherently deterministic. But since one of the primary features of our fault model is its ability to produce complex (perhaps chaotic) solutions, one could ask whether earthquake prediction is possible in principle since chaotic systems are notorious for their sensitive dependence on initial conditions (e.g., *Thompson and Stewart* [1987] or *Moon* [1987]).

Predictions of the long-term future behavior of the fault system will probably depend sensitively on the measured condition of the fault. However, for a useful prediction, one may only care about the next cycle of activity. A measurement of the fault state (with some finite precision) might lead to approximate predictions about the subsequent motions of the fault. However, it is not clear whether the time scale for information loss is the same as the time scale for a large earthquake cycle. Perhaps, instead, the time scale for information loss corresponds to the time scale of microseismic events. This latter contingency seems especially possible if an appropriate $\mathcal{D}$ is large. Like meteorological forecasts, near term prediction based on a dynamical model might be fairly accurate at some time scale with longer-term predictions correspondingly less accurate. *Horowitz* [1988*a*] addresses related issues using some of the techniques of chaotic dynamics.

Low-Speed Slip Between Events

One property of the friction law used here is that a fault system continues to slide very slowly during the intervals

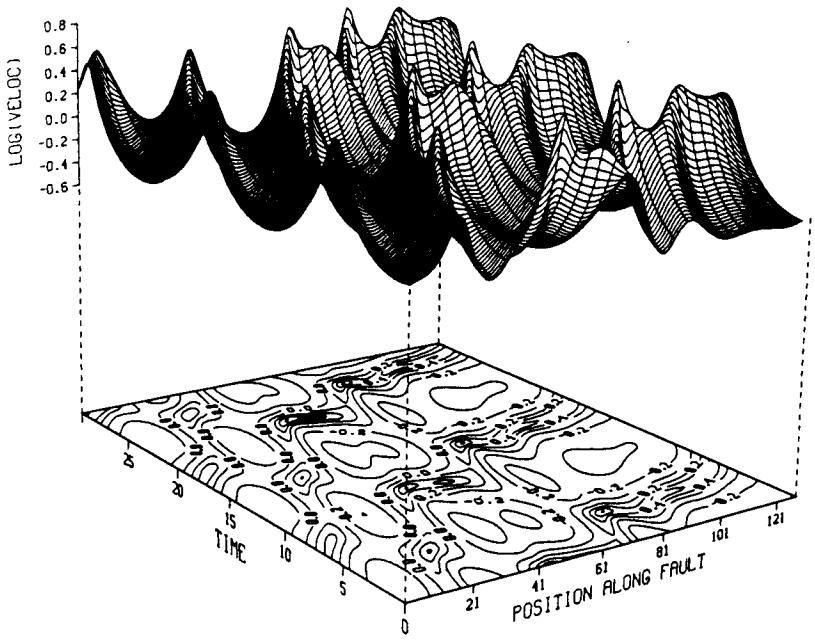

Fig. 10*a*. A perspective plot of a few cycles from a complex solution. $L/H\pi = 20$, $\mathcal{D} = 1.125$ This solution has a region (near node 12) that slips at nearly the driving velocity (a line parallel to the time axis at node 10 only crosses the 0 contour). Also, it has multiple event centers (at about nodes 21, 35, 45, 81, and 101) that are isolated from one another in both space and time. Creeplike waves propagate along certain regions of the fault (e.g., a creeplike wave moves from about node 110 wrapping around to about node 10 and then subsides).

between activity. Whether lack of field observation of slip in apparently locked regions represents a failure in the particular friction law being used, or a detection threshold, or both, is a somewhat academic question. It is possible to construct friction laws with similar structure to (1) that do make sense at zero slip rate and that would probably predict similar dynamical behavior to that presented here.

Accelerating Slip and Creep Events

In the complex motions reported here, accelerating slip or a propagating creep event always precedes rapid slip. Propagating creep events commonly appear as parts of solutions, (e.g., Figure 9*a*). Events propagate in either direction at a rate that depends on parameter values and also on the state of the fault before the event. The greatest slip rates are found to occur when and where two creep events collide. We do not know the relation between these propagating creep events and the steady but unstable creep waves of Figure 6.

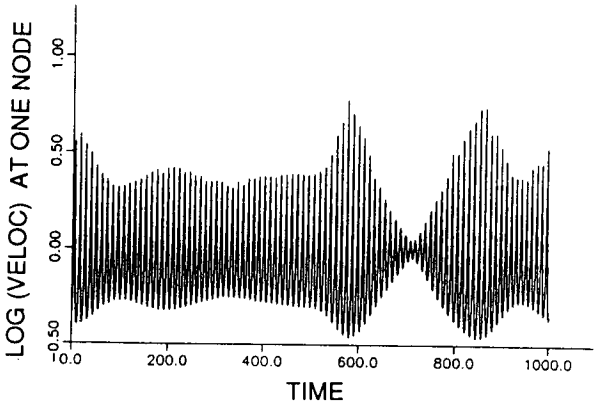

Fig. 10*b*. The aperiodic amplitude envelope for velocity of slip fluctuations for the same simulation as Figure 10*a*. Note the longer time scale.

Heterogeneities Not Needed to Localize Events

The complicated solutions that we have found in our simple model come from the dynamics of the system. Only unrealistically symmetrical initial conditions give simple solutions. The complicated, perhaps chaotic [*Horowitz* 1988*a*], solutions indicate that earthquake patterns may be as natural to fault slip as (chaotic) turbulence is to fluid flow. While the geometry and boundary conditions of our model are clearly oversimplified, the results show that an event need not be located at some special location along strike. We also demonstrate repetitive events whose spatial proximity might be misinterpreted as occurring at a strong patch since, in this model, locations of repetitive events are not mechanically distinct from neighboring locations.

Heterogeneous Properties Inhibit Complex Solutions?

In the calculations of *Mavko* [1980, 1983, also unpublished manuscript, 1984], *Tse and Rice* [1986], and *Stuart* [1988], strong heterogeneity (with depth) was assumed for the fault properties. In all of these solutions the final character of seismicity seems to be a stable limit cycle with fairly simple spatial structure. Comparing those simulations with the simulations here, it seems that spatial complexity in motion might be inhibited by heterogeneity in properties and encouraged by smoothness in properties. It seems possible that the spatial symmetry of our model contributes to

the complexity of the solutions. Thus it may be that the heterogeneity of fault structure does not always make slip dynamics complex, but in some ways contributes to keeping earthquake slip patterns simple, possibly suppressing results of the type shown here.

SUMMARY

A variety of spatially and temporally varying solutions are found from a simple homogeneous model. Phenomena which may be considered geophysically suggestive include creep waves and an overall complexity of fault activity. In our simulated earthquake process, we see event centers which seem to behave something like what one may observationally call asperities or strong patches. But unlike the common picture of large-scale asperities these centers are sometimes seen to be created, to migrate, and to disappear over many cycles.

APPENDIX 1: SOME TERMINOLOGY

The word instability is used in the contexts of dynamical systems and earthquake mechanics to have various different meanings many of which are relevant to the discussion here.

A solution to a set of differential equations is said to be (asymptotically) stable if, subsequent to any small perturbation from that solution, the solution is asymptotically reapproached. Otherwise the solution is unstable. Most often this definition is applied to solutions that are constant in time, such as constant rate slip in a spring block model. In these cases the stability analysis generally involves study of solutions to autonomous linear differential equations. Such analysis has been performed by, e.g., *Rice and Ruina* [1983] for steady slip solutions using rate and state friction laws and is discussed in the text.

However, a periodic or quasi-periodic solution can also be asymptotically stable or unstable depending on whether or not all small perturbations asymptotically reapproach that solution. Stability analysis of nonconstant solutions is generally much more difficult, and few results are known about state variable frictional systems. Periodic motions that are stable are called stable limit cycles. Most classical models of stick slip are descriptions of stable limit cycles. An unstable periodic motion is called an unstable limit cycle only if there are no other periodic motions that are infinitesimally close.

The definition of asymptotic stability just presented is equivalent to linear stability except in the special cases where linear stability analysis is indeterminate.

A model or system of differential equations is said to be structurally unstable if some qualitative feature it predicts (e.g., the existence or nonexistence of limit cycles) would disappear if the governing equations were changed infinitesimally.

In contrast to the dynamical uses of instability just discussed, motion that is observed when sliding is unsteady (e.g., stick slip) is often loosely called "unstable motion." However such motion can itself be asymptotically stable if it persists after small perturbations.

In common usage, a sudden motion or event is termed an instability. In some earthquake models this definition can be made precise: instability is when the ratio of the slip rate to the controlled boundary rate becomes infinite. This infinite ratio generally coincides with a point in the deformation process at which not all of the governing equations can be satisfied. However, in models that use sufficiently rate-dependent material properties, or that include inertia, this definition of instability becomes somewhat arbitrary. From a seismological point of view, one would like to define motion associated with seismic signals as instabilities. However, this definition requires the distinction of an arbitrary threshold in some measure of event size (slip rate, moment, etc.) in order to separate creep events, accelerating slip, creep after events, etc., from instabilities. We use the words slip event rather than instability to describe motions that are relatively fast compared to some kind of average.

APPENDIX 2: NUMERICAL SOLUTION METHOD

The various slip variables (τ, θ, V, δ are calculated at N (=8, 32, 128, 512, or 1024) nodes on the frictional surface (Figure 1*b*). Each node (labeled by the subscript i) must satisfy the friction law and is elastically coupled to every other node. The node spacing measured as a physical distance in Figure 1*b* depends on the dimensionless model variable $L/H\pi$, the number of nodes N, and the overall length scale H (i.e., dimensional distance between nodes is $L/N = H\pi(L/H\pi)/N$).

There are a number of ways that the discretized problem can be written as $2N$ coupled first-order autonomous ordinary differential equations in time. There is also some choice in the independent variables to be used in the calculations. It seems most natural to use the total slip $\hat{\delta}$ as one of the independent variables. However, our simulations have very large slip distances, and the elasticity calculation would then require the numerically dangerous subtraction of large, nearly equal numbers (the slip displacement $\hat{\delta}$ and the load point displacement $\hat{V}_0 t$). We chose to use $\hat{\theta}$ as one independent variable so the same program could be used with two state variables in the friction law (though no two state variable simulations are presented here). For illustrative purposes we explain our time stepping method using $\hat{\tau}$ as the other independent variable. One may be helped in understanding the physical model and the governing equations by thinking through the Euler's method solution below. We have

$$\hat{\theta}_i(\hat{t}+\Delta\hat{t}) = \hat{\theta}_i(\hat{t}) + \dot{\hat{\theta}}_i(\hat{t})\,\Delta\hat{t} \quad \text{(A1)}$$

$$\hat{\tau}_i(\hat{t}+\Delta\hat{t}) = \hat{\tau}_i(\hat{t}) + \dot{\hat{\tau}}_i(\hat{t})\,\Delta\hat{t} \quad \text{(A2)}$$

and the auxiliary equations

$$\hat{V}_i(\hat{t}+\Delta\hat{t}) = \exp[\hat{\tau}_i(\hat{t}+\Delta\hat{t}) - \hat{\theta}_i(\hat{t}+\Delta\hat{t})] \quad \text{(A3)}$$

$$\hat{\delta}_i(\hat{t}+\Delta\hat{t}) = \hat{\delta}_i(\hat{t}) + \hat{V}_i(\hat{t})\Delta\hat{t} \quad \text{(A4)}$$

where i ranges from 1 to N. The right-hand sides of (A1) and (A2) can be evaluated from the values of $\hat{\theta}$ and $\hat{\tau}$ at the previous time step $\hat{t}$ using (8) as follows. In (A1), $\dot{\hat{\theta}}_i(\hat{t})$ is found from direct application of (8*b*) using $\hat{V}_i(\hat{t})$ and $\hat{\theta}_i(\hat{t})$. The term on the right-hand side of (A2), $\dot{\hat{\tau}}$, is found from the elasticity solution (8*c*) using the values of $\hat{V}$ at all of the nodes. Equation (A3) is (8*a*) solved for $\hat{V}_i$. Equation (A4) for $\hat{\delta}_i$ is only needed for display purposes. With the solution (A1) and (A2), $\hat{\delta}_i$ is not independent and could have been found (with greater accuracy and greater computational cost) using the values of $\hat{\tau}_i$, $\hat{V}_0\hat{t}$ and the Fourier transform elasticity solution instead of with (A4).

Evaluation of the right-hand side of (A2) requires solution of the elasticity equations (8) at every time step. We use the fast Fourier transform (FFT) as a truncated approximation to an exact Fourier series solution. The computation time with this algorithm is proportional to $N \log N$ as contrasted with an N^2 proportionality when using a Green's (influence) function superposition and resulting matrix multiplication. The FFT is used with the $K(\kappa)$ supplied by the sine wave elasticity solutions described in the text.

The time stepping method we actually used, a two-point Runge-Kutta (midpoint) method (described in any numerical methods text) is very similar to the Euler's method description just given. Also, we used V as an independent variable rather than τ. The time steps were automatically adjusted during integration and are typically limited so that no node slips more than $0.05d_c$ to $0.1d_c$ per time step or changes its slip rate by more than 5–10%. Both of these conditions are needed since parts of the solutions involve very rapid slip and parts have large changes in slip rate over small slip distances. These conditions on the time steps are an approximate way of imposing a formal bound on the numerical error in the time integration. When many nodes (e.g., 1024) were used, the time step was further reduced to avoid numerical instabilities associated with "stiff" differential equations. (This numerical "stiffness" results from the high physical stiffness associated with the highest elastostatic modes.) We have tested the dependence of several representative solutions on the size of the time steps and found that convergence was reached (within the resolution of our graphical output) using time steps restricted as described.

NOTATION

A constant in friction law associated with direct rate dependence.
B constant in friction law associated with θ dependence on slip rate.
$\hat{B}$ normalized B, identical to B/A.
C constant in friction law associated with θ's dependence on slip rate.
$\hat{C}$ normalized C, identical to C/A.
d_c constant in friction law, the characteristic slip displacement.
$\mathcal{D}$ dimensionless constant, $\mathcal{D} \equiv K_{crit}/K$ for a spring block and $\mathcal{D} \equiv K_{crit}/K_0$ for an elastic slab; $\mathcal{D}$ is a measure of system stability, $\mathcal{D} < 1 \Rightarrow$stability and $\mathcal{D} > 1 \Rightarrow$instability.
E Young's elastic modulus.
F Function in friction law.
G elastic modulus (Lamé shear constant) for isotropic elastic slab, also a function in friction law.
H thickness of elastic slab, represents distance to constant rate tectonic motion.
i node number on discretized frictional surface.
K stiffness ([stress]/[distance]) of a spring or of a slab for wave number κ.
$\hat{K}$ dimensionless K, identical to $Kd_c/\sigma A$.
K_0 stiffness K of slab when the whole length slips simultaneously, identical to $G/(2H)$.
$\hat{K}_0$ dimensionless K_0, identical to $Gd_c/(2\sigma AH)$.
K_n stiffness of slab for mode number n.
K_{crit} dimensionless parameter associated with the friction law (defined in equation (2a)), spring stiffness K is compared to K_{crit} by means of $\mathcal{D}$ to determine stability.
$\hat{K}_{crit}$ dimensionless K_{crit}, identical to $K_{crit}d_c/(\sigma A)$.
L length of the elastic slab, period of the periodic boundary condition.
N number of nodes used in the spatial discretization of the elastic slab's surface.
n the sinusoidal mode number under discussion, $0 \leq n \leq N/2$.
Q_1, Q_2 expressions used in sine wave elasticity solution (defined after equations (5) and (6)).
$\mathcal{T} \equiv \tanh(|\kappa|H)$, expression used in sine wave elasticity solution.
t time.
$\hat{t}$ dimensionless t, identical to $V_t t/d_c$.
$\hat{t}_0$ time offset, an arbitrary constant.
V slip rate between elastic slabs ($V = V(x,t)$), identical to $\dot{\delta}$.
$\hat{V}$ dimensionless V, identical to V/V_t.
V_0 constant in boundary condition for the slabs equal to relative average motion rate for slabs; driving speed in spring block model.
$\hat{V}_0$ dimensionless V_0, identical to V_0/V_t.
V_t constant in friction law, associated with transition from negative to positive steady state rate dependence.
x position along the fault.
$\hat{x}$ dimensionless x, identical to x/H.
$\hat{x}_0$ position offset, an arbitrary constant.
δ slip displacement of a block ($\delta = \delta(t)$), or relative slip displacement of slabs ($\delta = \delta(x,t)$).
θ state variable in the friction law, implicitly defined by equation (1b), $\theta = \theta(t)$ for block, $\theta = \theta(x,t)$ for slabs.
$\hat{\theta}$ dimensionless θ, identical to θ/A.
κ wave number of sine wave slip displacement on elastic slab.
κ_{crit} that κ whose associated stiffness is K_{crit}.
κ_{wave} wave number of the fundamental component of a simulated creep wave.
$\hat{\kappa}$ dimensionless κ, identical to $H\kappa$.
μ_0 constant in the friction law, the nominal coefficient of friction.
ν elastic constant of isotropic elastic slab, Poisson's ratio.
σ normal component of stress transmitted across slab interface, does not depend on x or t.
τ shear component of stress transmitted across slab interface, the friction stress, $\tau = \tau(x,t)$ for slabs.
$\hat{\tau}$ dimensionless τ, identical to $(\tau/(\sigma A) - \mu_0/A)$.
τ_{ss} steady state value of τ at a given V, defined in equation (1c).
ϕ phase of slip and of stress sine wave on elastic slab, defined implicitly in equation (3a).
$\Delta(\,)$ change in $(\,)$.
$\dot{(\,)}$ time derivative: $d(\,)/dt$ or $\partial(\,)/\partial\hat{t}$ or $d(\,)/d\hat{t}$ depending on context.

Acknowledgments. This paper includes work presented at the 1983 and 1985 Fall AGU meetings, and at the 1985 Ewing Symposium on earthquake source mechanics. We thank Les Schaffer,

Ernest MacMillan, Teng-fong Wong, John Rudnicki, Ross Stein, Jeff Nussbaum, Pamela Smith, Suresh Goyal, and two anonymous reviewers for comments on the text; H. Don Conway for providing the Marguerre reference and helping in its translation; Tim Healy and Richard Rand for discussion of nonlinear stability; and Rich Gates, Rick Cochran, and Mike Heisler for help with computing. The symbolic manipulation program MACSYMA was used to obtain the 2-D $K(\kappa)$. One of us (F.G.H.) appreciates employment provided by Larry Cathles during portions of the re-writing of this manuscript. This work was sponsored by the U.S. Geological Survey and the National Science Foundation.

REFERENCES

Andrews, D.J., Coupling of energy between tectonic processes and earthquakes, *J. Geophys. Res., 83*, 2259-2264, 1978.

Blanpied, M.L., T.E. Tullis, and J.D. Weeks, Frictional Behavior of Granite at Low and High Sliding Velocities, *Geophys. Res. Let.*, 14, 554-557, 1987.

Burridge, R. and L. Knopoff, Model and theoretical seismicity, *Bull. Seismol. Soc. Am., 57*, 341-371, 1967.

Cao, T., and K. Aki, Effect of slip rate on stress drop, *Pure Appl. Geophys., 124*, 515-529, 1986.

Dieterich, J.H., Modeling of rock friction, 1, Experimental results and constitutive equations, *J. Geophys. Res., 84*, 2161-2168, 1979*a*.

Dieterich, J.H., Modeling of rock friction, 2, Simulation of preseismic slip, *J. Geophys. Res., 84*, 2169-2175, 1979*b*.

Dieterich, J.H., Constitutive properties of faults with simulated gouge, in *Mechanical Behavior of Crustal Rocks, Geophys. Monogr. Ser.*, vol. 24, edited by N.L. Carter, M. Friedman, J.M. Logan and D.W. Stearns, pp. 103-120, AGU, Washington, D.C., 1981.

Dieterich, J.H., and G. Conrad, Effect of humidity on time-and velocity-dependent friction in rocks, *J. Geophys. Res., 89*, 4196-4202, 1984.

Gu, J.-C., J.R. Rice, A. Ruina, and S.T. Tse, Slip motion and stability of a single degree of freedom elastic system with rate and state dependent friction, *J. Mech. Phys. Solids, 32*, 167-196, 1984.

Horowitz, F.G., Complexities in fault activity from a laboratory derived friction law, Ph.D. thesis, Cornell Univ., Ithaca, N.Y., 1988*a*.

Horowitz, F.G., Mixed state variable friction laws: Some implications for experiments and a stability analysis, *Geophys. Res. Let., 15*, 1243-1246, 1988*b*.

Marguerre, K., Druckverteilung durch eine elastische schicht auf starrer rauher unterlage, *Ing. Arch., 2*, 108-117, 1931.

Mavko, G.M., Simulation of creep events and earthquakes on a spatially variable model, *Eos Trans. AGU, 61*, 1120, 1980.

Mavko, G., Simulation of large-scale earthquake cycles by using a laboratory friction law, *Eos Trans. AGU, 64*, 851, 1983.

Moon, F.C., Chaotic vibrations: an introduction for applied scientists and engineers, 309 p., John Wiley, New York, 1987.

Nussbaum, J., and A. Ruina, Two degree of freedom earthquake model with static/dynamic friction, *Pure Appl. Geophys., 125*, 629-656, 1987.

Rice, J.R., and A. Ruina, Stability of steady frictional sliding, *J. Appl. Mech., 50*, 343-349, 1983.

Rice, J.R., and S.T. Tse, Dynamic motion of a single degree of freedom system following a rate and state dependent friction law, *J. Geophys. Res., 91*, 521-530, 1986.

Ruina, A.L., Slip instability and state variable friction laws, *J. Geophys. Res., 88*, 10, 359-10, 370, 1983.

Ruina, A.L., Constitutive relations for frictional slip, in *Mechanics of Geomaterials*, edited by Z.P. Bazant, pp. 169-187, John Wiley, New York, 1984.

Stuart, W.D., Forecast model for great earthquakes at the Nankai trough subduction zone, *Pure Appl. Geophys., 126*, 619-641, 1988.

Thompson, J.M.T., and H.B. Stewart, *Nonlinear Dynamics and Chaos: Geometrical Methods for Engineers and Scientists*, 376 pp., John Wiley, New York, 1987.

Tse, S. T., and J.R. Rice, Crustal earthquake instability in relation to the depth variation of frictional slip properties, *J. Geophys. Res., 91*, 9452-9472, 1986.

Tullis, T. E. (Ed.), *Friction and Faulting*, Birkhäuser, Stuttgart, 1987. (Also *Pure Appl. Geophys., 124*, 375-381, 1986.)

Weldon, R.J., II, and K. E. Sieh, Holocene rate of slip and tentative recurrence interval for large earthquakes on the San Andreas fault, Cajon Pass, southern California, *Geol. Soc. Am. Bull., 96*, 793-812, 1985.

F. G. Horowitz, Department of Civil Engineering, Technological Institute, Northwestern University, Evanston IL 60208.

A. L. Ruina, Department of Theoretical and Applied Mechanics, Thurston Hall, Cornell University, Ithaca, NY 14850.

(Received: February 1, 1988;
revised: September 12, 1988;
accepted: September 14, 1988.)